AAC Shear Wall Specimens:
Development of Test Setup and Preliminary Results

by

Matthew John Brightman, B.S.C.E

THESIS

Presented to the Faculty of the Graduate School of

The University of Texas at Austin

in Partial Fulfillment

of the Requirements

for the Degree of

Master of Science in Engineering

The University of Texas at Austin

May 2000

AAC Shear Wall Specimens:
Development of Test Setup and Preliminary Results

Approved by
Supervising Committee:

Supervisor: Richard E. Klingner

Michael E. Kreger

Dedication

This thesis is dedicated with love and thanks to my mom and dad, who have given me so much along the way.

Acknowledgements

The funding for this research was provided by the AACA. I would like to thank everyone involved at the AACA who contributed to the research.

I would like to show my appreciation to Dr. Richard Klingner for all the time he spent working with me and the rest of the "AAC Mafia" during the course of the project. I would like to also thank my coworkers, Jennifer Tanner and Jorge Varela, for all of their hard work and for putting up with me. I would also like to acknowledge their contributions to Chapters 1, 2, and 4 of this thesis.

I would also like to thank Dr. Michael Kreger for being my second reader and the "Thesis Crew" who made it bearable to sit in front of a computer for so many hours. Thank you to all those in the lab who provided assistance during construction. I want to specifically thank Blake Stasney, Wayne Fontenot, Mike Bell, and Ray Madonna for putting up with our many, many questions.

A special thanks goes to Dr. David McLean at Washington State University who provided me so many opportunities while I was there. Without his support, I would probably not have considered graduate school.

Finally, a thanks goes out to my family and friends. Dad, Mom, Mark, Grandma, Grandpa, Grammie, and Gramps, your support and praise was much appreciated and kept me going. Thanks to my "rent-a-brother," Bryan, and friend Terry for showing me how to have a good time. If it were not for them, I do not think I would still be sane.

May 5, 2000

Abstract

AAC Shear Wall Specimens:
Development of Test Setup and Preliminary Results

Matthew John Brightman, M.S.E

The University of Texas at Austin, 2000

Supervisor: Richard E. Klingner

The specimens tested for this thesis are the first and second of a series of AAC shear walls being tested under the auspices of the AACA. The overall objective of the test series is to develop behavioral models that can form the basis for code-type design provisions for AAC elements and systems in seismic zones. The specimens presented in this thesis are pilot specimens for the project used to develop construction techniques, improve testing procedures, and acquire preliminary results used to improve behavioral models. The behavior of the specimens is summarized and the implications of that behavior are reviewed.

Table of Contents

List of Tables

List of Figures

CHAPTER 1: INTRODUCTION

1.1 GENERAL

The growing use of Autoclaved Aerated Concrete (AAC) throughout the United States has brought with it a need for research on this building system's seismic performance. Over the past decade, the threat of seismic activity has recently been introduced to some areas of the United States that were formerly perceived as non-seismic. For example, the areas around St. Louis, Missouri and Charleston, South Carolina have recently been changed from areas with very little perceived seismic risk to areas with a higher potential for seismic activity. The need for further research also comes from the desire to expand the AAC market into areas of the United States where seismic risk is significant.

Some research has been completed on the seismic performance of AAC shear walls. Most of this research has focused on the behavior of walls made out of AAC masonry-sized blocks. For example, one research project performed lateral tests on wallettes made of AAC blocks (de Vekey 1986); another tested the flexural behavior of non-load bearing AAC walls (Al-Shaleh 1997). Other research addresses the behavior and bearing capacity of AAC walls with confining concrete elements (Dimitrov 1997), and the capacity of AAC masonry walls with out-of-plane and axial loads (Gerber-Balmelli 1994).

Based on the literature search conducted as part of this study, no research has yet addressed the effects of panel orientation on the behavior of AAC shear walls. Additionally, there is insufficient research on the seismic behavior of AAC

to develop seismic design provisions. Sufficient information, however, has been acquired to permit the development of design provisions in areas with little seismic risk, such as Florida and Texas.

The research described in this thesis forms part of a research program supported by the Autoclaved Aerated Concrete Association (AACA). The program is being carried out at the Phil M. Ferguson Structural Engineering Laboratory of The University of Texas at Austin. Its purpose is to fill in many of the gaps that exist in the present knowledge of AAC behavior.

1.2 SCOPE OF STUDY

The goal of the research funded by the AACA is to produce seismic design provisions for autoclaved aerated concrete. Results of the study at the University of Texas at Austin along with studies being completed at other institutions, will form the basis for design equations, including the necessary R and C_d factors.

The study at the University of Texas at Austin comprises at least two phases, with an optional third phase. Phase I consists of a series of tests on AAC shear walls of varying aspect ratios, with and without axial load. Phase I comprises twelve AAC shear wall specimens with aspect ratios ranging from 0.62 (behavior dominated by shear) to 3.08 (behavior dominated by flexure). The specimens will be constructed using a variety of panels and block orientations, reinforcement layouts, and axial loads. Results from these tests will be used to

develop design provisions for AAC shear walls, diaphragms, pier elements, cladding, and frame infills.

Phase II of the study involves testing an assemblage to verify the results of Phase I in application. The assemblage will be a single-bay, three-story structure loaded laterally in two perpendicular directions. The structure will include floors and walls, with and without openings for doors and windows, which will be used to test the validity of the equations developed during Phase I. The assemblage will also be used to verify the integrity of connection details similar to those now used in concrete and masonry construction.

If the connection details do not perform as expected, the optional Phase III will be completed. Phase III would involve a series of tests to improve current connection details and the design equations predicting their behavior. After the improvements are made, another assemblage would be tested to verify connection performance.

1.3 OBJECTIVES OF STUDY

The objectives of the study being completed at the University of Texas at Austin are to:

- establish basic procedures for predicting the diagonal cracking strength of AAC walls and wall elements as a function of aspect ratio and axial load;
- verify basic procedures for predicting the shear strength of vertically reinforced AAC walls and wall elements as a function of aspect ratio and vertical reinforcement;

- verify basic procedures for predicting the flexural behavior of flexurally reinforced AAC walls as a function of axial load and vertical reinforcement;
- verify the differences in behavior of AAC shear walls with the same overall geometry, but with different arrangements and amounts of minimum prescriptive reinforcement. Some specimens will have minimum reinforcement at the ends of the wall only. Other specimens will have maximum reinforcement, consisting of internal reinforcement in horizontally-oriented panels combined with supplementary vertical reinforcement in reinforced concrete elements;
- determine the differences in behavior of AAC shear walls with the same overall geometry, reinforcement, and axial load, but with different orientations of panel and block elements;
- verify that current connection details for conventional concrete and masonry are applicable in AAC construction; and
- combine many of the elements tested into a single AAC assemblage, to test the interaction among AAC elements and verify the proposed design provisions.

The results from the University of Texas at Austin study will be combined with other research being completed, and will be used to develop seismic design provisions that will enable AAC to be used throughout the United States and in other countries of the western hemisphere.

1.4 SCOPE OF THESIS

This thesis focuses on the in-plane behavior of shear walls constructed of horizontal AAC panels. The specimens addressed in this thesis were constructed with panels without additional site-installed reinforcement, and without significant axial load. For the thesis, two pilot specimens were constructed. These pilot specimens were used to develop the construction skills necessary to build AAC walls, to test and improve the loading and data acquisition systems, and to acquire preliminary information about the behavior of shear-dominated AAC shear walls.

The wall specimens were designed so that their behavior would be dominated by shear. The two specimens are described in Chapter 3 and the results from the tests are described in Chapters 4 and 5.

1.5 OBJECTIVES OF THESIS

The objectives of this thesis are to:

- develop and improve construction techniques;
- develop and improve testing procedures; and
- evaluate behavior of shear-dominated AAC shear walls constructed of horizontal panels.

1.6 ORGANIZATION OF THESIS

This thesis describes the testing process and results from the subset of the research program described above. Chapter 2 gives a more complete description

of the research background, of AAC itself, and of the construction process. The testing program is described in Chapter 3. The geometry and panel layout of the specimens, loading equipment, instrumentation, and data acquisition system are all described in that chapter. Results for the two pilot tests are presented in Chapters 4 and 5, and their significance is presented in Chapter 6. Chapter 6 also discusses recommendations for future research based on the observed behavior. Finally, Chapter 7 summarizes the results and presents major conclusions.

CHAPTER 1: BACKGROUND

1.1 DESCRIPTION OF AUTOCLAVED AERATED CONCRETE

Autoclaved Aerated Concrete (AAC), also known as cellular concrete, is a lightweight cellular material, most commonly composed of portland cement, quicklime, and finely ground sand. Some or all of the sand and cement can be replaced by fly ash. In the most common method of production, the dry materials are mixed with water to form a slurry, which is poured into large open molds. As the slurry is poured, it is mixed with a small amount of gas-forming agent, usually finely powdered aluminum. The aluminum powder reacts with the alkaline cement, forming many microscopic bubbles of hydrogen gas, which cause the slurry to increase in volume. At the same time, the quicklime reacts with the water to form hydrated lime, giving off considerable heat in the process. This heat is sufficient to produce an accelerated initial set in the portland cement within a few hours. The resulting "cake" is strong enough to support its own weight, and retains the cellular structure produced by the hydrogen bubbles. The cake is then de-molded, and cut into the desired shapes. At this stage of curing, the cake can be cut relatively easily, using steel wires. The cut shapes are then cured in an autoclave, producing a final material with about the same density as wood and which can be easily cut and shaped with hand tools (RILEM 1993).

Specifications for large panel units have been developed by ASTM Committee C-27 (ASTM C1386), and specifications for AAC masonry units are under development in ASTM Committee C-15.

1.1.1 Panel Types

AAC is produced in a variety of shapes and sizes. Products manufactured include masonry blocks, floor and roof panels, wall panels, staircase steps, lintels, and curtain walls, in a variety of lengths and thickness. The typical thickness of the blocks and panels ranges from 4 in. (102 mm) to 12 in. (305 mm). The masonry blocks are usually 8 in. (203 mm) tall and 24 in. (610 mm) long. Floor, roof, and wall panels are typically 24 inches tall (610 mm) and have a maximum length of 240 inches (6.10 m), but can be easily cut to shorter lengths.

1.1.2 Properties of AAC

AAC is typically divided into classes based on compressive strength. Each manufacturer has developed its own classes and corresponding specified properties. Similar to conventional portland cement concrete, many of the properties of AAC vary with the mix or class (Table 2-1).

Table 2-1: Ranges of typical AAC properties for two principal US manufacturers

Property	Ytong (Ytong 1999)			Hebel (Hebel 1999a)		
	AC2	**AC4**	**AC6**	**AAC 2.5**	**AAC 5.0**	**AAC 7.5**
Compressive Strength, psi (MPa)	345 (2.4)	570 (3.9)	855 (5.9)	360 (2.5)	725 (5.0)	1090 (7.5)
Dry Density, pcf (kg/m^3)	25 (400)	31 (500)	40 (650)	32 (515)	38 (610)	44 (700)
Modulus of Elasticity, 10^3 psi (MPa)	190 (1300)	260 (1800)	360 (2500)	246 (1700)	326 (2250)	384 (2650)
Thermal Expansion Coefficient	4.4 (8)	4.4 (8)	4.4 (8)	4.5 (8)	4.5 (8)	4.5 (8)
Thermal Conductivity, BTUin./ft^2h°F (W/mK)	0.80 (0.11)	0.97 (0.14)	1.25 (0.18)	0.96 (0.14)	1.15 (0.16)	1.15 (0.16)

1.1.3 Properties of Thin-Bed Mortar

The thin-bed mortar used to bond the AAC panels is more like a structural adhesive than a conventional masonry mortar. It is typically laid only in joints that are approximately 1/32 to 1/8 inch (1 to 3 mm) thick. It is made from a mix of portland cement, fine silica sand, polymers such as latex or vinylester, and admixtures such as water-retention admixtures. The mortar is designed so that it

will be stronger than the AAC itself. For example, the range of compressive strengths specified for the mortar is 1160 to 1450 psi (8.0 to 10 MPa), which is greater than the maximum compressive strength of the AAC (Ytong 1999)[1].

1.2 CONSTRUCTION PROCESS

The general construction process is independent of whether horizontal panels, vertical panels or blocks are used. First, the top of the concrete base or foundation is roughened by light bush-hammering, and shims are placed on top, level to within a tolerance of ±1/32 inch (0.8 mm). Next, a portland cement-lime masonry mortar is placed on top of the floor beam between the shims (Figure 2-1). The masonry mortar used in the tests for this thesis conformed to ASTM C270, Type S by proportion, with some thin-bed mortar added to enhance tensile bond strength and to help retain water. The shims and mortar provide a surface on which to level the first course of panels.

[1] Personal communication, Texas Contec, 1999.

Figure 2-1: Combination of Type S mortar and thin-bed mortar on floor beam

Since the first course is level, the blocks are manufactured to close tolerances, and the mortar joints are quite thin, it is not necessary to level subsequent courses. Subsequent courses are laid over the preceding one with only a layer of thin-bed mortar separating them (Figure 2-2).

Figure 2-2: Placing horizontal panel during construction

If the wall is constructed of vertical panels, each panel must be individually leveled. This requires placing leveled shims at each side of each panel and placing the conventional mortar on the base around the shims. The most critical panel is the first one. It is carefully plumbed. The following panels are set on their own shims and then clamped against the previously placed panel. These can be assumed to be plumb because of the tight tolerances in the panels. Figure 2-3 shows the placement of a vertical panel.

Figure 2-3: Placing vertical panels during construction

In a wall constructed of AAC masonry units, the first course of units is the only one that must be leveled. As with the large panels, the leveling bed consists of leveled shims for each individual block plus the conventional masonry mortar between the shims. Subsequent courses need not be leveled.

The thin-bed mortar is placed using a special trowel designed specifically for this. The trowel has a large area for scooping mortar, and large teeth on the

end, used to distribute evenly the mortar by controlling its thickness across the whole panel or block. The mortar is applied to horizontal and vertical joints to provide continuity between all adjacent blocks (Figure 2-4).

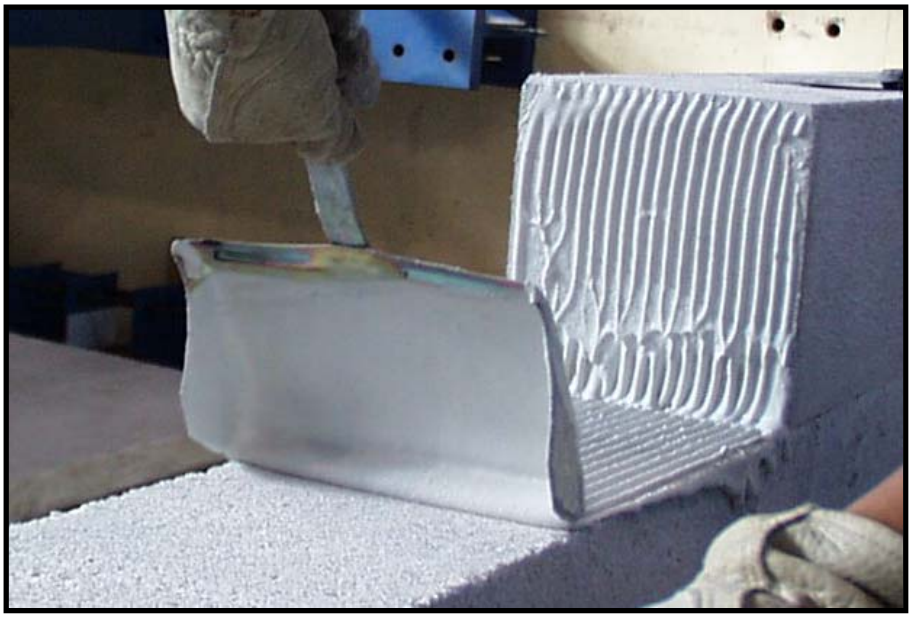

Figure 2-4: Laying thin-bed mortar with special trowel

1.3 BACKGROUND ON SEISMIC DESIGN

Current United States seismic design codes assign values of R (force reduction factor) and C_d (drift amplification factor), and prescriptive reinforcement requirements, based on a combination of technical justification, politics and tradition. In the new *International Building Code* (IBC 2000), the R values assigned to masonry are lower (by about ½) than the values for concrete.

For example, the *R* value for a particular system made of masonry might be 2-½, while the *R* value for the same system, in concrete, would be about 3.

For this reason, if AAC is classified as masonry, it will automatically be penalized in terms of seismic design base shear. Code values for *R* and C_d should be based on the combination of material behavior and the structural system, rather than on the material per se and the structural system. If AAC behaves like concrete, it should be so classified for purposes of assigning *R* and C_d values, regardless of whether the structural configuration is achieved using large panels or using small, masonry-type units.

If design of AAC is based on working-stress principles, it will irrationally but inevitably be perceived as insufficiently reliable to be designed by strength principles. For that reason, it is probably better to work from the very beginning for AAC design approaches that are consistent with strength design of concrete and strength design of masonry, using the new IBC.

1.4 MAJOR EVENTS IN RESPONSE OF SHEAR WALLS TO LATERAL IN-PLANE LOADS

The behavior of a concrete or masonry shear wall subjected to in-plane lateral loading can be viewed as a sequence of "major events" -- significant changes in stiffness, strength or appearance (particularly cracking). Those major events are listed below, not necessarily in order of occurrence:

- flexural cracking;
- web shear cracking;

- flexural shear cracking;
- yielding of shear reinforcement;
- yielding of extreme flexural reinforcement;
- nominal flexural capacity; and
- sliding shear failure.

These major events may not all occur during a single test. The events that do occur, and level of applied loading at which each occurs, depend on the wall's geometry, material properties, reinforcement, amount of axial load, and loading history.

1.5 DESCRIPTION OF EXISTING METHODS FOR CALCULATING LATERAL CAPACITY AT MAJOR EVENTS

To compute the lateral capacity corresponding to each major event for AAC shear walls, it is useful to draw on background material related to the behavior of similar elements that have been more extensively tested in the laboratory and in actual applications of shear walls of reinforced concrete or masonry. That background material is reviewed in this section.

Notation

A_n net cross-sectional area of wall

A_s area of longitudinal tension reinforcement in wall segment

A_v area of shear reinforcement within a distance s

A_{vf} area of shear-friction reinforcement

c distance from extreme compression fiber to neutral axis

d distance from extreme compression fiber to centroid of tension reinforcement

f'_{AAC} specified compressive strength of ACC

f_c compressive strength of concrete

f'_c specified compressive strength of concrete

f_m compressive strength of masonry

f'_m specified compressive strength of masonry

f_t tensile strength of material

f_y yield strength of reinforcement

h total height of wall from base to point of load application

l_w length of entire wall in direction of shear force

M design moment

M_{cr} moment causing flexural cracking at a section due to externally applied loads

M_n nominal moment strength at section

n normal stress

N design axial load normal to cross section occurring simultaneously with V; to be taken as positive for compression and negative for tension

s spacing of shear reinforcement in direction parallel to longitudinal reinforcement

S_x elastic section modulus of section

t thickness of wall

v shear stress

V design shear force at section

V_c nominal shear strength provided by concrete

V_{cr} shear causing flexural cracking at a section

V_m nominal shear strength provided by masonry

V_n nominal shear strength

V_s nominal shear strength provided by shear reinforcement

V_{ss} nominal sliding shear capacity

V_y shear causing yield of longitudinal reinforcement

β_1 empirical factor used to calculate depth of Whitney Stress Block (equivalent stress block) as a percentage of c

μ coefficient of friction

σ maximum flexural tensile stress

1.5.1 Flexural Cracking

For reinforced concrete and masonry, flexural cracking occurs as shown in Figure 2-5 when the flexural tensile stress in the wall exceeds the tensile capacity of the concrete (Equation 2-1).

$$\frac{M}{S_x} \pm \frac{N}{A_n} > f_t \qquad (2\text{-}1)$$

Where the moment is equal to

$$M = V \cdot h \qquad (2\text{-}2)$$

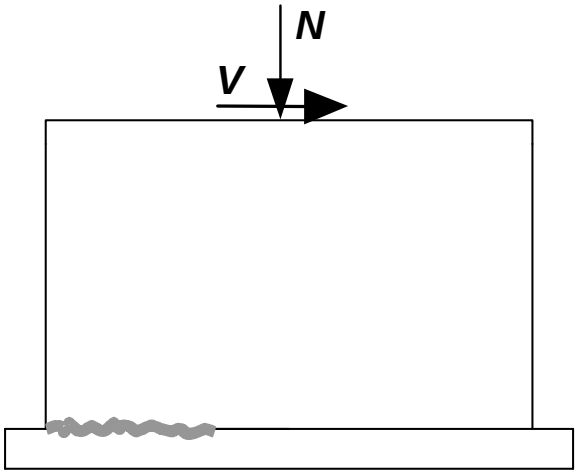

Figure 2-5: Flexural crack

By rearranging Equation 2-1, the corresponding shear at which flexural cracking occurs is given by Equation 2-3:

$$V_{cr} = \frac{\frac{tl_w^{\,2}}{6}\left(f_t + \frac{N}{tl_w}\right)}{h} \qquad (2\text{-}3)$$

1.5.2 Web Shear Cracking for Reinforced Concrete Shear Walls

For reinforced concrete shear walls, one possible mode of shear cracking is the formation of an inclined crack near the center of the wall. This type of cracking is called web shear cracking and is shown in Figure 2-6.

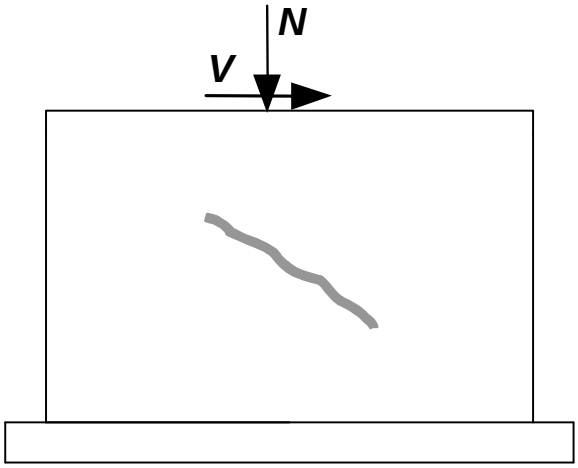

Figure 2-6: Web shear cracking

This inclined crack forms when the principal tensile stress in the web exceeds the tensile strength of the concrete. The principal stress is given by Equation 2-4, where the normal stress in the wall is *n* and the maximum shear stress in the center of the web is *v*.

$$f_t = \sqrt{\left[\left(\frac{n}{2}\right)^2 + \left(v^2\right)\right]} - \frac{n}{2} \quad \text{where} \quad v = \frac{3V}{2l_w t} \quad \text{and} \quad n = \frac{N}{l_w t} \qquad (2\text{-}4)$$

Substituting the values for *n* and *v* and solving, the corresponding shear capacity, V_c, is given by Equation 2-5.

$$V_c = \frac{2l_w t}{3} f_t \cdot \sqrt{1 + \left(\frac{N}{f_t l_w t}\right)} \qquad (2\text{-}5)$$

The *ACI Building Code* (ACI 1999), Equation 11-31, uses a conservative (low) tensile capacity of $4\sqrt{f_c'}$. The effective depth, *d*, the distance between the compression centroid to the outermost layer of tension steel, is approximated as 80% of the length of the wall. This leads to Equation 2-6, a semi-empirical equation for web shear cracking:

$$V_c = 3.3td\sqrt{f_c'} + \frac{Nd}{4l_w} \qquad (2\text{-}6)$$

1.5.3 Flexural Shear Cracking for Concrete Shear Walls

A flexural shear crack begins as a horizontal flexural crack, and propagates diagonally. A fully developed flexural shear crack will begin at a height above the base of about one-half the plan length of the wall, l_w, as shown in Figure 2-7.

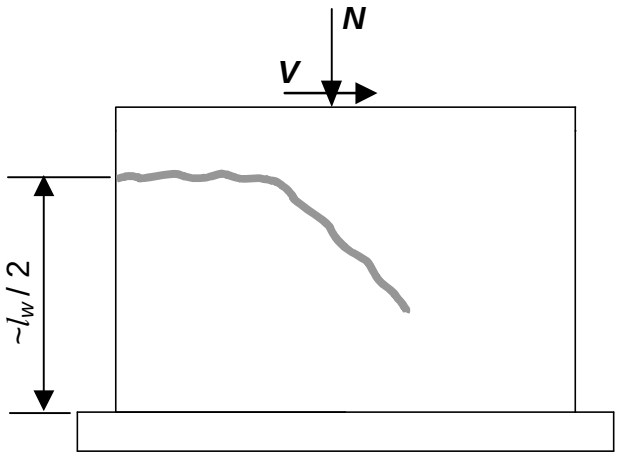

Figure 2-7: Flexural shear cracking

The formation of this crack is governed by the maximum flexural tensile stress in the wall (Equation 2-7).

$$\sigma = \frac{M}{S_x} \pm \frac{N}{A_n} \qquad (2\text{-}7)$$

Based on experiments, the controlling crack develops at a height of about $l_w/2$. Therefore, the moment that occurs at the crack, M_{cr} is:

$$M_{cr} = M - \frac{Vl_w}{2} \qquad (2\text{-}8)$$

where M is the moment at the base.

Substituting Equation 2-8 into Equation 2-7 and solving for the shear, V, results in the semi-empirical Equation 2-9. The *ACI Building Code* (ACI 1999) uses a conservative (low) flexural tensile strength, f_t, of $6\sqrt{f_c'}$; experiments have shown that an additional force of $0.6\sqrt{f_c'} \cdot td$ is required to develop the crack.

$$V_c = \frac{S_x \cdot \left(f_t + \frac{N}{l_w t} \right)}{\left(\frac{M}{V} - \frac{l_w}{2} \right)} + 0.6 \cdot \sqrt{f_c'} \cdot td \qquad (2\text{-}9)$$

The *ACI Building Code* (ACI 1999) uses the following equation for the flexural shear cracking capacity.

$$V_c = \left[0.6\sqrt{f_c'} + \frac{l_w\left(1.25\sqrt{f_c'} + 0.2\frac{N}{l_w t}\right)}{\frac{M}{V} - \frac{l_w}{2}} \right] \cdot td \qquad (2\text{-}10)$$

1.5.4 Shear Cracking of Masonry Shear Walls

Equations 2-6 and 2-10, developed for web shear cracking and flexural shear cracking of concrete walls, could also be applied to masonry walls. The *International Building Code* (IBC 2000) provisions for masonry, however, use a single empirical equation for the cracking shear capacity of masonry walls (Equation 2-11).

$$V_m = \left[4 - 1.75 \cdot \left(\frac{M}{Vl_w} \right) \right] \cdot A_n \sqrt{f_m'} + 0.25N \qquad (2\text{-}11)$$

1.5.5 Yielding of Shear Reinforcement

After the formation of a diagonal crack, shear capacity comes from aggregate interlock and dowel action from vertical reinforcement, plus the tensile capacity of the shear reinforcement. The contribution from the concrete is presumed to be at least equal to the shear required to cause cracking (the smaller of the values for web shear cracking and flexural shear cracking but greater than $2ht\sqrt{f_c'}$). The nominal shear capacity, V_n, is the sum of the resistance provided by the concrete and by the yielded shear reinforcement (Equation 2-12).

$$V_n = V_c + V_s \qquad (2\text{-}12)$$

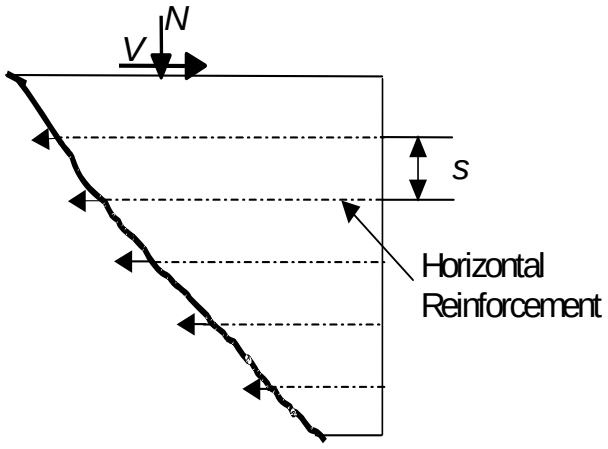

Figure 2-8: Yielding of shear reinforcement

V_s provided by the shear reinforcement is given by Equation 2-13.

$$V_s = \frac{A_v f_y d}{s} \qquad (2\text{-}13)$$

If the height of the wall is less than d, d should be replaced by h.

1.5.6 Nominal Flexural Capacity for Concrete and Masonry Shear Walls

Assuming that plane sections remain plane, nominal flexural capacity can also be predicted based on conventional flexural analysis of the wall. The compressive zone is determined based on a linear strain relationship, using a maximum useful compressive strain of 0.003 (RILEM 1993) in the AAC, and an equivalent rectangular stress block whose height is $0.85f'_{AAC}$ (or $0.85f'_c$, or $0.85f'_m$), and whose depth is $\beta_1 c$, where $\beta_1 = 0.85$ (Figure 2-9).

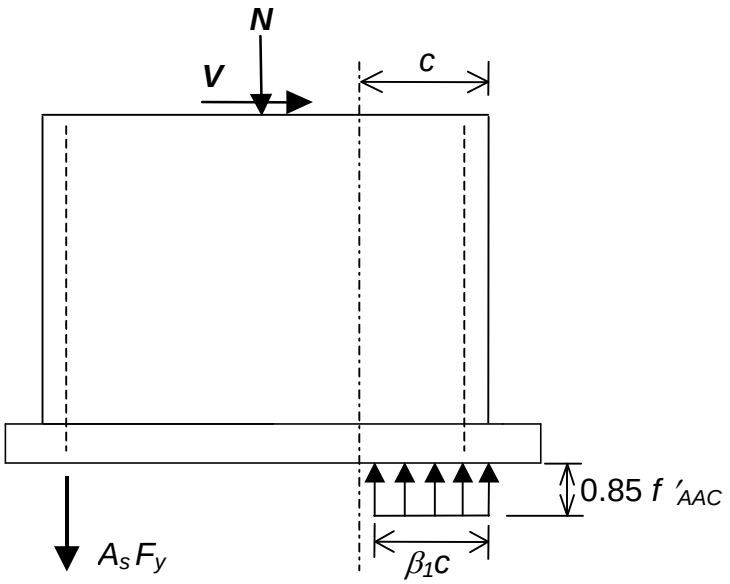

Figure 2-9: Flexural theory applied to walls at M_n

For the case with reinforcement only at the ends of the wall, the nominal shear capacity can be calculate using equilibrium of the section (Equation 2-14).

$$V_n = \frac{A_s f_y (d - \frac{\beta_1 c}{2})}{h} \qquad (2\text{-}14)$$

More generally, Cardenas and Magura (Cardenas 1973) showed that from equilibrium, the lateral capacity in this state for a wall with uniformly distributed reinforcement is expressed by Equation 2-15.

$$V_n = \frac{\frac{1}{2} A_s f_y l_w \cdot \left(1 + \frac{N}{A_s f_y}\right) \cdot \left(1 - \frac{c}{l_w}\right)}{h} \qquad (2\text{-}15)$$

Equation 2-15 can be used as an approximation to the lower portion of a moment-axial force interaction diagram like that shown in Figure 2-10. Interaction diagrams can be developed for first yield and for nominal capacity.

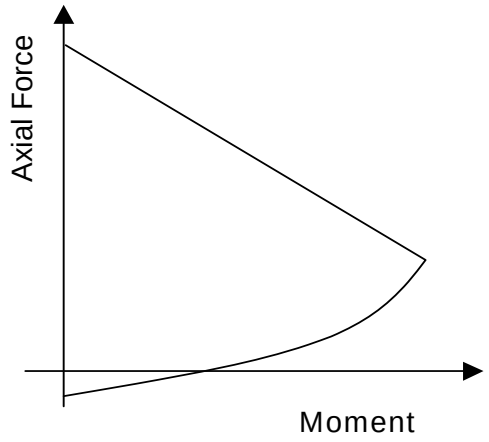

Figure 2-10: Schematic moment-axial force interaction diagram for AAC shear wall

1.5.7 Yielding of Extreme Flexural Reinforcement

The horizontal force at which the longitudinal reinforcement yields may be determined based on flexural theory, as illustrated in Figure 2-11.

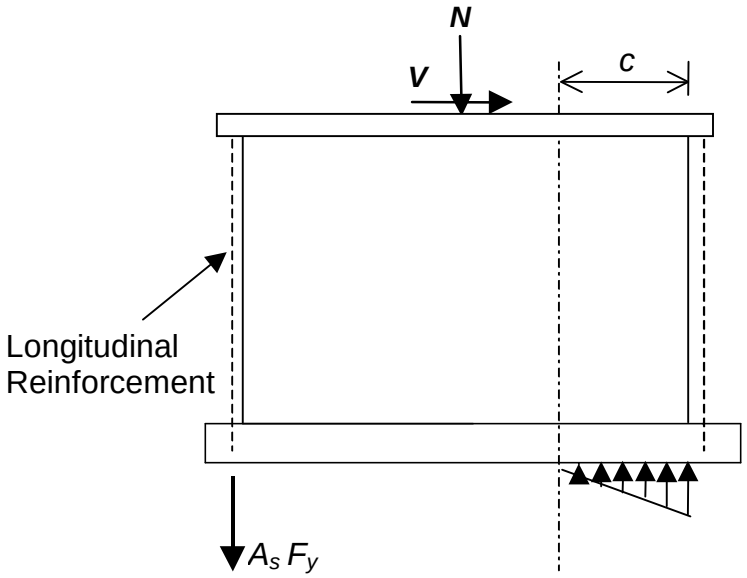

Figure 2-11: Flexural theory applied to shear wall pilot specimens at yielding of reinforcement

By equilibrium, the compressive force in the concrete is equal to the tensile force in the reinforcement plus the applied axial load. The area of the compressive stress block may be determined based on an assumed linear variation of strain. The resulting applied shear required to yield the flexural reinforcement can be determined based on flexural equilibrium (Equation 2-16):

$$V_y = \frac{A_s f_y}{h}\left(d - \frac{c}{3}\right) - \frac{N}{h}\left(\frac{l_w}{2} - \frac{c}{3}\right) \qquad (2\text{-}16)$$

1.5.8 Sliding Shear Failure

An AAC shear wall will exhibit a bed-joint crack when the shear stress between panels exceeds the initial interface shear capacity, v, or when the tensile capacity across a joint is exceeded.

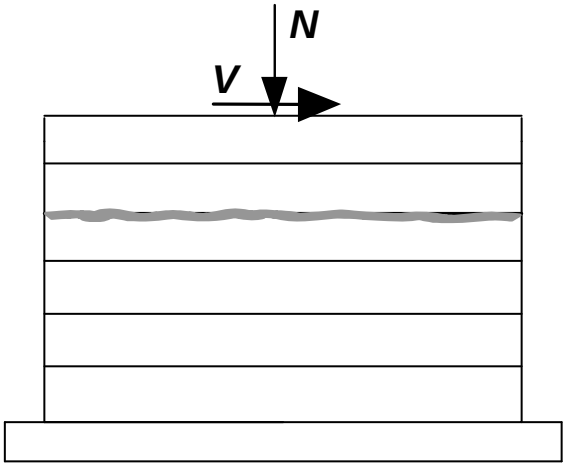

Figure 2-12: Formation of crack at bed joint

After the crack forms, the resistance across the bed joints provided by shear friction, V_{ss}, can be calculated using Equation 2-17.

$$V_{ss} = \mu \cdot (A_{vf} \cdot f_y + N) \qquad (2\text{-}17)$$

Under reversed cyclic loading, the roughness of the bed joints can decrease, which decreases the coefficient of friction, μ. As a result, the sliding shear capacity can be controlled by dowel action of reinforcement crossing the

bed joints. This resistance V_{ss} is given by Equation 2-18, and the resistance mechanism is presented in Figure 2-13.

$$V_{ss} = \mu \cdot N + A_{vf} \cdot 0.6 \cdot f_y \qquad (2\text{-}18)$$

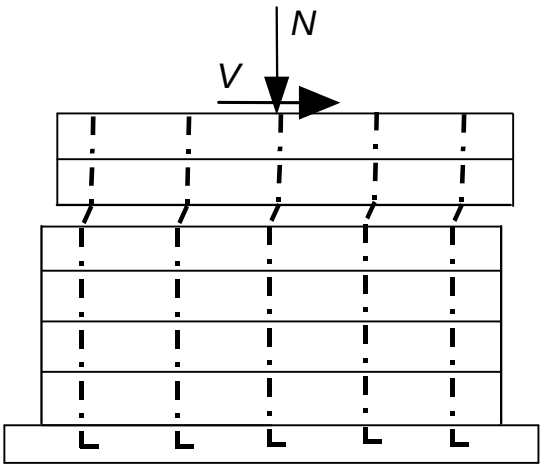

Figure 2-13: Sliding shear mechanism

1.5.9 Summary of Applied Shear Corresponding to Each Major Event

From above formulas it can be seen that the lateral capacity of a concrete or masonry shear wall depends on the values of material compressive strength (f_c or f_m), axial load (N), and ratio of bending moment to shear force. The applied shear required to cause each major event can be estimated using the formulas in Table 2-2.

Table 2-2: Summary of applied shear corresponding to each major event

MAJOR EVENT	APPLIED SHEAR
flexural cracking	$\frac{\frac{tl_w^{\,2}}{6}\left(f_t+\frac{N}{tl_w}\right)}{h}$
web shear cracking	$\frac{2l_wt}{3}f_t\cdot\sqrt{1+\left(\frac{N}{f_tl_wt}\right)}$
flexural shear cracking	$\frac{S_x\cdot\left(f_t+\frac{N}{l_wt}\right)}{\left(\frac{M}{V}-\frac{l_w}{2}\right)}+0.6\cdot\sqrt{f_c'}\cdot td$
shear cracking of masonry walls	$\left[4-1.75\cdot\left(\frac{M}{Vl_w}\right)\right]\cdot A_n\sqrt{f_m'}+0.25N$
yielding of shear reinforcement (force carried by shear reinforcement at nominal shear strength)	$A_v\cdot f_y\cdot\frac{d}{s}$
yielding of flexural reinforcement	$\frac{A_sf_y}{h}\left(d-\frac{c}{3}\right)-\frac{N}{h}\left(\frac{l_w}{2}-\frac{c}{3}\right)$
nominal flexural strength	$\frac{\frac{1}{2}f_yl_w\cdot\left(1+\frac{N}{A_sf_y}\right)\cdot\left(1-\frac{c}{l_w}\right)}{h}$
sliding shear (shear friction) capacity	$\mu\cdot(A_{vf}\cdot f_y+N)$
sliding shear (dowel action) capacity	$V_{ss}=\mu\cdot N+A_{vf}\cdot 0.6\cdot f_y$

1.5.10 Expected Behavior

The expected behavior of the AAC shear wall specimens was calculated using the above formulas as shown in Appendix A. For the pilot specimens in this thesis, the first anticipated major event was flexural cracking. This was predicted to decrease the stiffness of the wall, signified by the first change in slope in Figure 2-14. The next expected major event was web shear cracking. At that point, the wall was expected to begin to degrade at the web shear crack, and to decrease in stiffness and strength, as shown by the descending portion in Figure 2-14. As shown in the figure, the wall was never expected to reach yielding of longitudinal reinforcement.

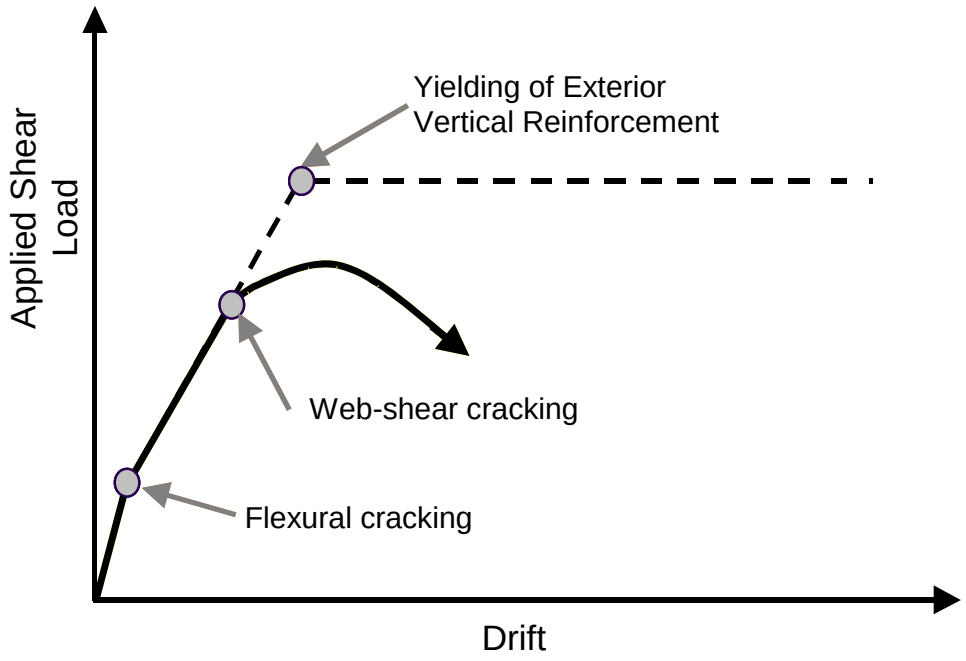

Figure 2-14: Expected behavior of AAC shear wall pilot specimens

The pilot specimens did experience a change in stiffness after flexural cracking, which concurred with the predictive model. A shear force large enough to cause web shear cracking, however, could not be applied. The inability to force web shear cracking was due to inexperience in construction techniques and difficulties in getting load into the AAC wall without inducing high local stress concentrations. The actual behavior and problems mentioned above are described thoroughly later in this thesis.

CHAPTER 1: TEST PROGRAM

This thesis addresses a series of in-plane tests on AAC shear walls. In this chapter the test setup for those tests, objectives of each test, characteristics of each test specimen, loading equipment, instrumentation, and loading history are described.

1.1 OBJECTIVES OF TESTING PROGRAM

The shear wall specimens described here were intended to represent AAC shear walls whose behavior is controlled by shear rather than flexure. The specimen geometry and loading were selected based on that objective.

1.2 TEST SPECIMENS

Two test specimens were used in the tests described here. Both were pilot specimens used to test the construction techniques, loading equipment, instrumentation, and data acquisition systems. Shear Wall Pilot Specimens 1 and 2 were constructed of horizontal panels.

1.2.1 Shear Wall Pilot Specimen 1

Shear Wall Pilot Specimen 1 was made of horizontal AAC panels oriented in running bond (Figure 3-1). The specimen measures 20 ft (0.61 m) long by 12.33 ft (0.376 m) high (top of base to level of load application) by 8 in. (203

mm) thick. Its aspect ratio (height divided by plan length) is 0.62. The AAC material, thin-bed mortar, and construction supervision were supplied by Contec Mexicana (Monterrey, Mexico).

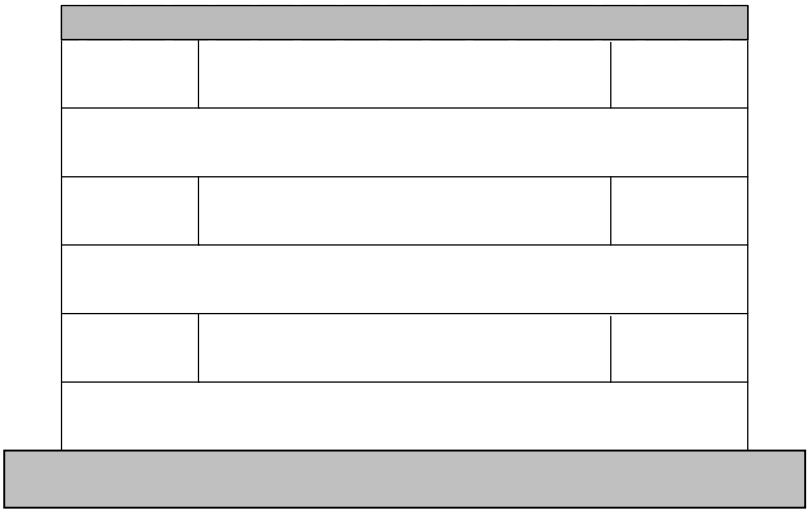

Figure 3-1: Layout of Shear Wall Pilot Specimen 1 and 2

1.2.2 Shear Wall Pilot Specimen 2

The layout of Shear Wall Pilot Specimen 2 is the same as that of Shear Wall Pilot Specimen 1 (Figure 3-1), with the only difference being the construction techniques. Based on results from the first pilot test, Shear Wall Pilot Specimen 2 was constructed under the supervision of Matrix Precast Autoclaved Aerated Concrete (Smyrna, Georgia). The AAC panels were supplied by Contec Mexicana and the thin-bed mortar was supplied by Ytong Florida, Ltd.

(Haines City, Florida). The construction procedure was modified to increase the bond between panels by applying the thin-bed mortar in a different way. Reasons for this modification in construction procedure, and details of it, are given later in this thesis.

1.3 TEST SETUP

1.3.1 Lateral Loading System

Lateral load is applied using two horizontal actuators mounted side-by-side (Figure 3-2), connected at one end to two steel channels bolted along the top of the specimen, and at the other end to Ferguson Laboratory's biaxial reaction wall. The applied load is transferred to the wall specimen through friction, created by evenly spaced post-tensioned bolts clamping the channels to the specimen.

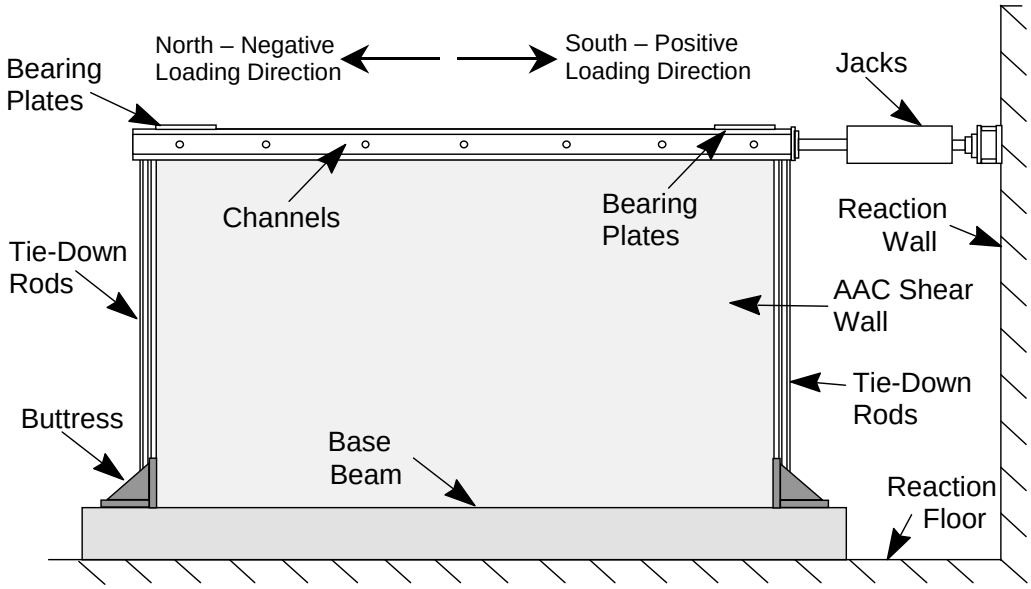

Figure 3-2: Setup for applying lateral load

1.3.2 Base Beam

The specimen sits on a precast concrete base beam (Figure 3-2), representing a concrete foundation. The specimen is connected to the base beam using conventional portland cement-lime masonry mortar conforming to ASTM C270, Type S by proportion, with some thin-bed mortar added to enhance tensile bond strength and to retain water. To prevent the specimen from sliding or uplifting, the base beam is bolted to the reaction floor using post-tensioned rods.

1.3.3 Tie-Down Rods

To increase the in-plane flexural capacity of the specimens under in-plane loads, and thereby encourage shear-dominated behavior, the specimens were anchored to the base beam using two external tie-down rods, 1 in. (25 mm) in diameter, at each end of the specimen.

1.3.4 Bearing Plates

The tie-down rods are connected to the channels at the top of the wall through integral bearing plates, whose purpose is to prevent the channels from moving vertically downward under the tie-down force.

1.3.5 Buttresses to Prevent Sliding

Since flexural cracks were expected to form at the base of the specimens and increase the tendency for in-plane sliding shear at the base, buttresses were attached to the base beam at each end of the specimen to prevent in-plane sliding (Figure 3-2), while keeping contact stresses below the crushing strength of the AAC.

1.3.6 Out-of-Plane Bracing

The specimen is braced against out-of-plane displacement by cables, one end of which is attached to vertically-oriented rods welded to the channels at two points on both sides of the wall, and the other end of which is attached to

horizontally-oriented rods bolted through holes in the flanges of W-shape columns positioned alongside the specimen (Figure 3-3) and bolted to the reaction floor.

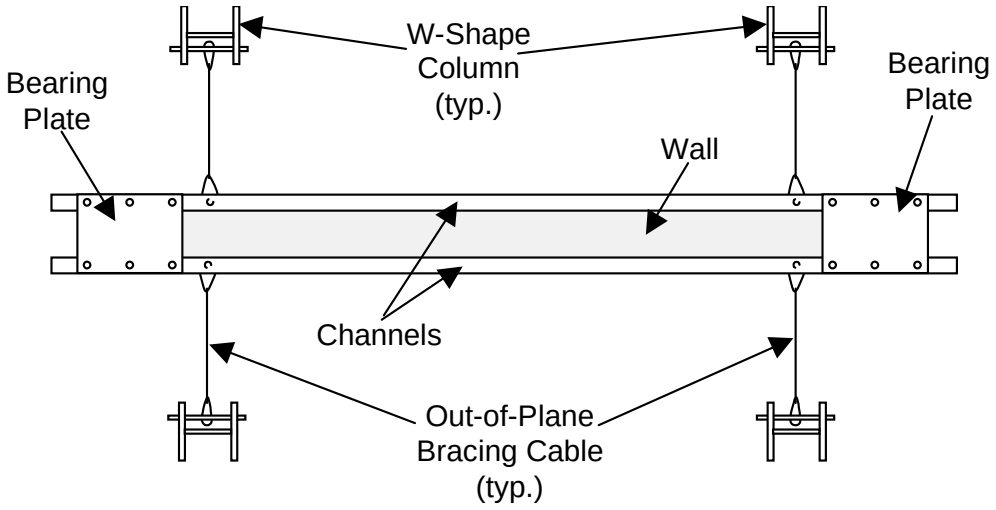

Figure 3-3: Lateral bracing system (plan view)

1.4 INSTRUMENTATION AND DATA ACQUISITION

1.4.1 Instrumentation used to Determine Overall Behavior

The instrumentation used to determine overall hysteretic behavior (Figure 3-4) includes:

- load cells to measure the applied horizontal shear force;

- pressure transducers to measure the pressure in the jacks that applied the horizontal force. This pressure value is converted to an applied force and is used as a check on the load cells;
- linear potentiometers to measure the horizontal displacement at the top of the wall; and
- linear potentiometers to measure the full-height vertical displacement at the ends of the wall.

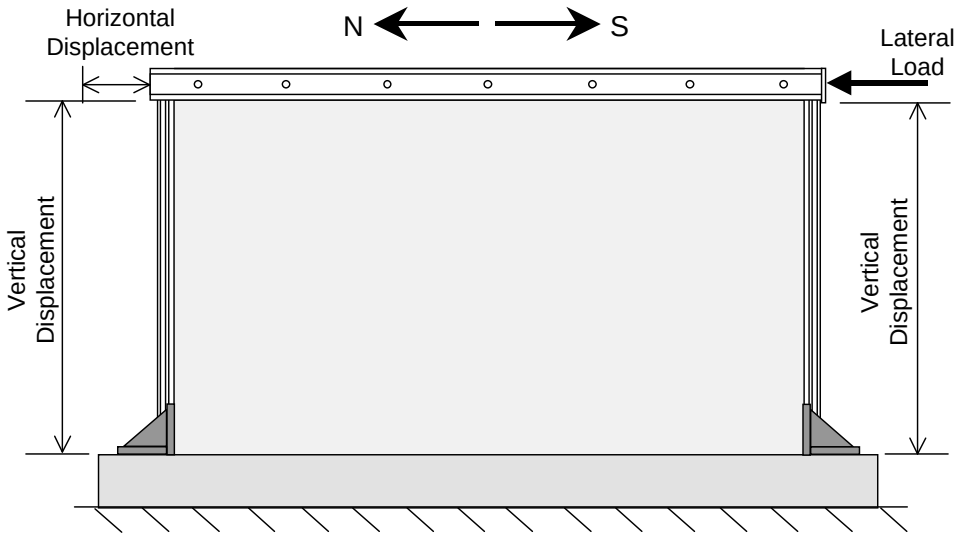

Figure 3-4: Instrumentation for measuring overall behavior

1.4.2 Instrumentation Used to Determine Local Behavior

The instrumentation used to determine local behavior (Figure 3-5) includes:

- linear potentiometers to measure:

- deformation across the diagonals of the specimen;
- incremental vertical deformations at the ends of the specimen;
- slip between the specimen and its base;
- slip between the base and the floor;
- slip between the channels and the top of the wall; and

- force washers to measure force in tie-down rods.

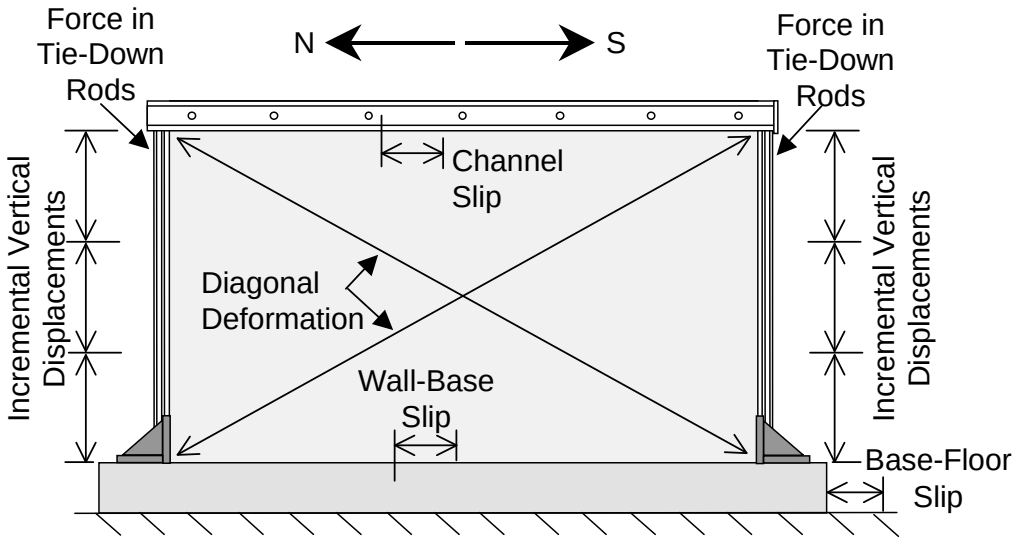

Figure 3-5: Instrumentation for measuring local behavior

1.4.3 Data Acquisition

Data were acquired through a Hewlett-Packard 3852 scanner. Analog-to-digital conversion was carried out by a National Instruments card in a Windows-based microcomputer, running under Measure, a National Instruments add-on for the Microsoft Excel spreadsheet program. Once in Excel format, data were plotted conventionally.

The instrumentation described in Sections 1.4.1 and 1.4.2 comprised twenty-four channels. The channels and their associated instrumentation are listed in Table 3-1.

Table 3-1: Instrumentation

Channel	Instrument	Measurement
100	10-volt voltmeter	Excitation
101	5-inch string potentiometer	north bottom third vertical displacement
102	5-inch string potentiometer	north middle third vertical displacement
103	5-inch string potentiometer	north top third vertical displacement
104	5-inch string potentiometer	south bottom third vertical displacement
106	5-inch string potentiometer	south top third vertical displacement
107	5-inch string potentiometer	north top-south bottom diagonal displacement
108	5-inch string potentiometer	south top-north bottom diagonal displacement
109	15-inch string potentiometer	north full-height vertical displacement
110	15-inch string potentiometer	south full-height vertical displacement
111	5-inch string potentiometer	south middle vertical displacement
112	15-inch string potentiometer	horizontal displacement
114	5000-psi pressure transducer	compression pressure in jacks
115	5000-psi pressure transducer	tension pressure in jacks
117	2-inch linear potentiometer	east channel-wall slip
118	2-inch linear potentiometer	west channel-wall slip
119	2-inch linear potentiometer	wall-foundation slip
201	150-kip load cell clevis pin	force in west jack
202	63-kip load cell force washer	force in south exterior tie-down rod
203	63-kip load cell force washer	force in south interior tie-down rod
204	63-kip load cell force washer	force in north interior tie-down rod
205	63-kip load cell force washer	force in north exterior tie-down rod
206	150-kip load cell clevis pin	force in east jack
207	2-inch linear potentiometer	foundation-floor slip

1.5 LOADING HISTORY

The planned in-plane loading history for the shear wall specimens, shown in Figure 3-6, consisted of a series of reversed cycles to monotonically increasing maximum load or displacement amplitudes. At the beginning of the test, target

load values were used; later, target displacement values were used. The predetermined target values (PV) were based on the loads that were calculated to produce significant changes in the behavior of the specimen (for example, flexural cracking or web shear cracking). The planned loading history involved three cycles to each maximum force or displacement level.

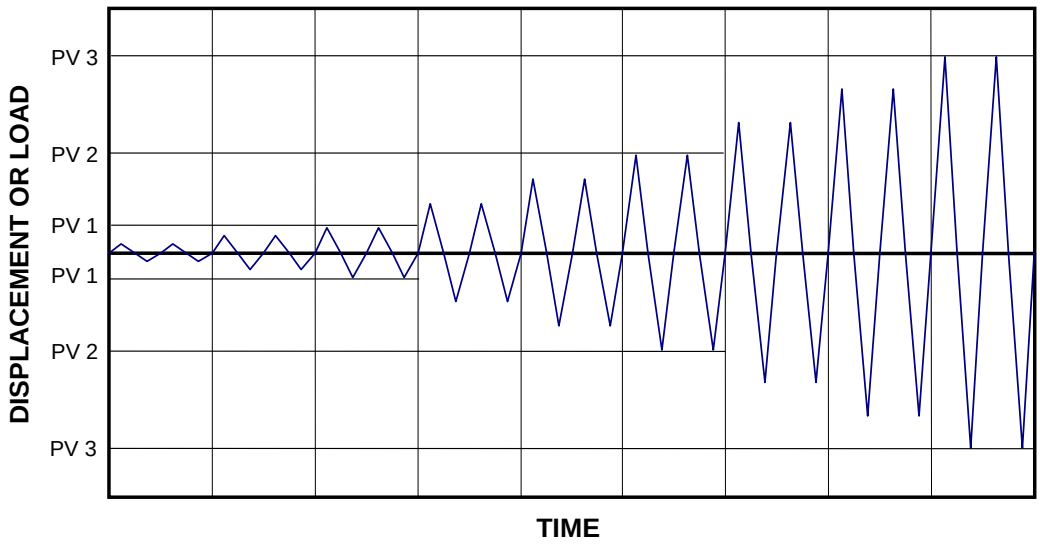

Figure 3-6: Planned loading history for shear wall pilot specimens

CHAPTER 1: RESULTS FROM TEST ON SHEAR WALL PILOT SPECIMEN 1

This chapter presents the results and behavior from the test on Shear Wall Pilot Specimen 1. In this section, the response of Shear Wall Pilot Specimen 1 is discussed, first with respect to load history, then with regard to the observed behavior and cracking patterns, and finally with respect to recorded load-displacement behavior. A complete list of the data collected during this test is presented in Section 3.4. Only those data necessary to describe the above results are presented here.

During the tests on both Shear Wall Pilot Specimen 1 and 2, calibration factors from the manufacturer were used for the load cells. The load cells measured the magnitude of the applied horizontal force at the top of the wall. Analysis of the data showed significant differences between the loads reported from the load cells and from the pressure transducers. Even though the pressure transducers had been calibrated prior to the tests, their output was not considered as reliable as the load cells, and they were mainly used as a check on the load cells. Therefore, the load cells were re-calibrated at the lab to check the manufacturer's calibration.

The re-calibration showed that the load cells were under-reporting the load by about 4%. This difference is relatively insignificant (about 1 kip, or 4.5 kN) at the levels used for the first two pilot tests. Therefore, data from this test were not modified to include the 4% increase. For future tests, however, the laboratory calibration factors will be used.

1.1 LOADING HISTORY

The planned loading history for Shear Wall Pilot Specimen 1 is shown in Figure 3-6. As was described in Chapter 3, the amplitudes of each cycle were established based on predicted major events. The predetermined load values for this specimen are shown in Table 4-1. An example of how these are calculated is shown in Appendix A.

Table 4-1: Predetermined values for Shear Wall Pilot Specimen 1

Predetermined Value (PV)	Major Event	Predicted Load
1	flexural cracking	22.3 kips (99.2 kN)
2	web shear cracking	55 kips (245 kN)
3	yielding of external flexural steel	185 kips (825 kN)

The actual load cycles from the tests are shown in Table 4-2, Figure 4-1, and Figure 4-2. The table and the figures break the data into cycles, identified at the top of Figures 4-1 and 4-2. Each cycle contains a number of load points at which data were recorded. For reference throughout this chapter, Table 4-2 shows which load points occurred during each cycle. The load points are identified by numbers that monotonically increase throughout the test. Loading to the south is considered to be positive, and is designated by an “a” next to the

cycle number. Loading to the north is said to be negative and is designated by a "b" next to the cycle number.

The drift ratios shown in the tables and figures below were adjusted for sliding of the wall along the base. Slip between the wall and the base was subtracted from the total displacement measured at the top of the wall. Histories for the base slip for both specimens are shown in Appendix B. The purpose of this correction was to isolate the behavior of the wall itself, so that an accurate drift ratio could be calculated.

The drift ratio is the specimen's in-plane horizontal displacement at the level of load application, divided by its height (the distance between the top of the base and the level of load application).

During the first part of the test, load was increased to predetermined force levels. An initial cycle was applied to a maximum load of 3 kips (13.3 kN) to make sure the instruments and data acquisition system were working; then sets of two full cycles were applied to maximum force levels of about 7, 15, and 22 kips (31.1, 66.7, and 89.0 kN respectively). The peak load and displacement values are shown in Table 4-2.

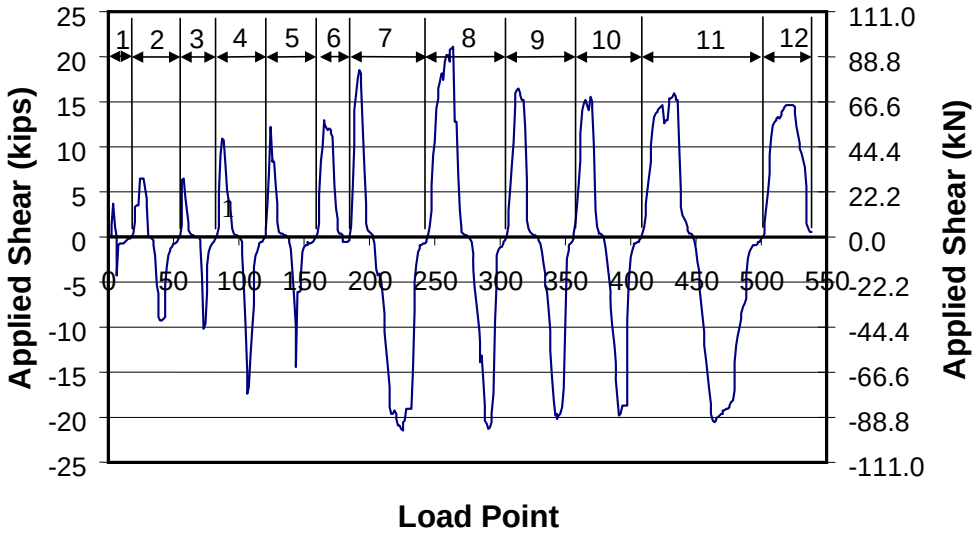

Figure 4-1: Actual loading history for Shear Wall Pilot Specimen 1 (numbers at top of plot designate cycle numbers)

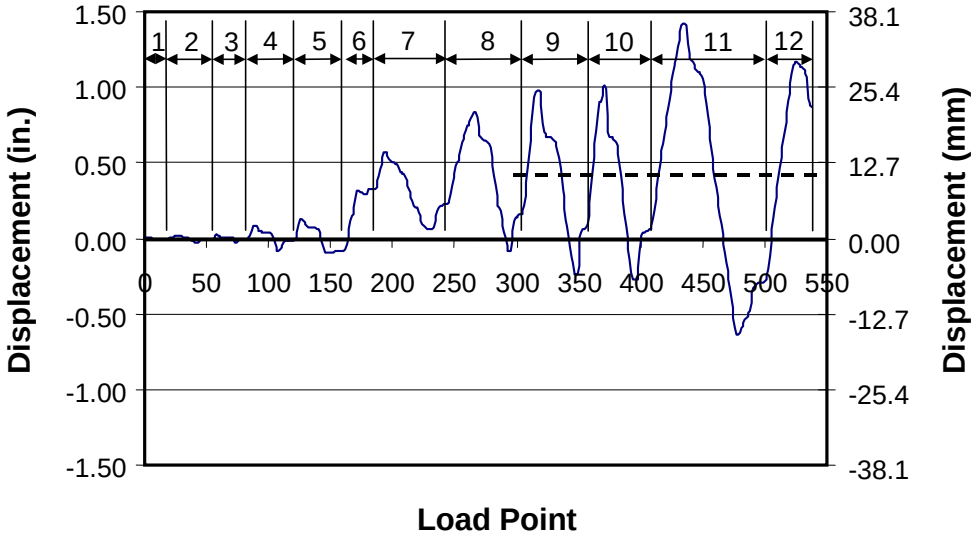

Figure 4-2: Actual displacement history for Shear Wall Pilot Specimen 1 (numbers at top of plot designate cycle numbers)

Table 4-2: Maximum load and drift ratio in each cycle for Shear Wall Pilot Specimen 1

Cycle	Load Points	Maximum Applied Load Kips (kN)	Maximum Drift Ratio
1a	1 - 6	3.6 (16.2)	0.005%
1b	7 – 18	-4.3 (-19.2)	-0.006%
2a	19 – 31	6.5 (29.0)	0.011%
2b	32 – 54	-9.3 (-41.3)	-0.016%
3a	55 – 68	6.5 (28.7)	0.012%
3b	69 – 82	-10.1 (-45.0)	-0.021%
4a	83 – 100	10.9 (48.5)	0.033%
4b	101 – 119	-17.4 (-77.4)	-0.046%
5a	120 – 137	12.3 (54.6)	0.049%
5b	138 – 159	-14.4 (-64.0)	-0.063%
6a	160 – 179	12.9 (57.6)	0.20%
6b	180 – 184	-0.5 (-2.1)	0.21%
7a	185 – 202	18.5 (82.1)	0.38%
7b	203 – 244	-21.4 (-95.2)	0.046%
8a	245 – 275	21.1 (93.7)	0.55%
8b	276 – 304	-21.2 (-94.3)	-0.048%
9a	305 – 328	16.5 (73.2)	0.64%
9b	329 – 356	-20.2 (-89.8)	-0.15%
10a	357 – 379	15.6 (69.2)	0.67%
10b	380 – 408	-19.8 (-87.9)	-0.17%
11a	409 – 448	15.9 (70.7)	0.95%
11b	449 – 500	-20.6 (-91.8)	-0.43%
12a	501 – 538	14.7 (65.2)	0.78%

Cycles 1 through 8 were force-based. During Cycle 6b, the load was decreased to zero after relative movement was detected across horizontal (bed) joints between panels, as described later in this chapter. At that point, additional

post-tensioning was applied into the external tie-down rods. The load was then increased again in the same direction to continue with the planned loading history.

At Cycle 8, examination of the real-time plot of base shear versus in-plane lateral displacement showed that the level of applied load was approaching the maximum predicted in-plane capacity of the wall. Therefore, the loading cycles were changed to displacement control. Displacement cycles of 0.6 in. (15 mm) and 1.0 in. (25 mm) were used in this test. Displacements were measured with respect to the permanent displacement offset of 0.4 in. (10 mm) that had already occurred during the force-based portion of the loading history. The dashed line in Figure 4-2 represents that permanent offset. Because that offset resulted from bed-joint sliding rather than wall deformation, it caused no stress in the AAC. Because that baseline corresponded to a zero-stress condition in the wall, it was used as the reference for imposing displacements during the rest of the test. The specimen was subjected to reversed cycles of monotonically increasing drift, arranged symmetrically with respect to that new reference.

Cycles 9 and 10 had maximum relative displacements of ±0.6 in. (±15 mm) from that new baseline. These displacements correspond to an in-plane lateral movement of +1.0 in. (+25 mm) and -0.2 in. (-5.0 mm) from the initial origin. Cycles 11 and 12 had maximum relative displacements of ±1.0 in. (±25 mm) from that new baseline, corresponding to total movements of +1.4 in. (+36 mm) and -0.6 in. (-15 mm) from the initial origin.

The wall failed during Cycle 12a, at a relative displacement of about 0.8 in. (20 mm) from the new baseline, corresponding to a total movement of about 1.2 in. (30 mm) from the initial origin.

1.2 SEQUENCE OF CRACK FORMATION

1.2.1 Flexural Cracking at Base

Before the test, shrinkage cracks had already formed along the base of the wall through the mortar joint (Figure 4-3). These cracks were the first to open during the test, and appeared as flexural cracks in the tension side of the wall during Cycles 3a and 3b.

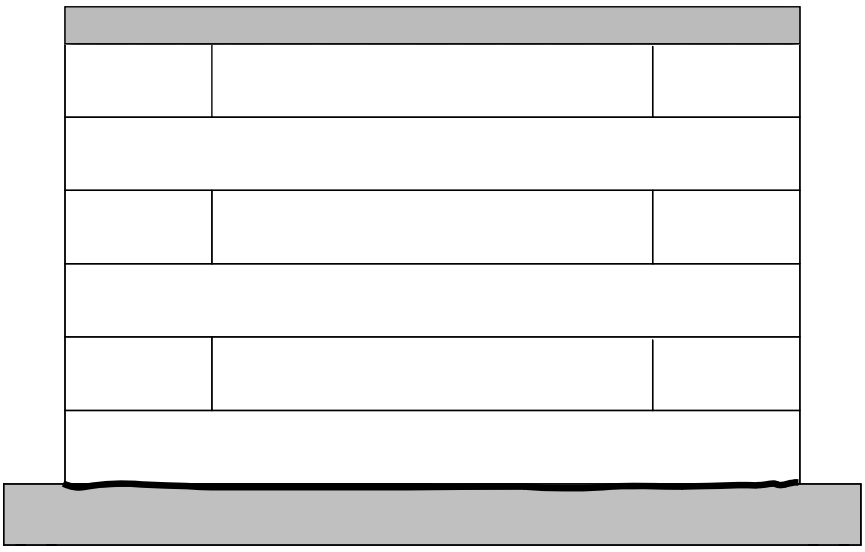

Figure 4-3: Initial shrinkage crack at base of Shear Wall Pilot Specimen 1

1.2.2 Bed-Joint Cracking

The next crack to form was a horizontal crack underneath the second panel from the top (Figure 4-4). In that and the following figures, black lines represent new cracks and gray lines represent pre-existing cracks. This crack indicated failure of the mortar joint under combined shear and tension.

The tension existed because of overall flexure, and because the buttresses did not allow the wall to rotate. As the wall was loaded in-plane, friction between the hydrostone and the buttress produced a hold-down force that created vertical tension along the end of the wall. During Cycles 5a and 5b, loud "pops" were heard, and were attributed to the wall slipping up the buttress. This tension, along with the poor bond between panels (described in Chapters 5 and 6) produced the bed-joint crack shown in Figure 4-4.

After this crack had formed, only friction resisted the sliding of the overlying portion of the wall. In-plane shear capacity as governed by friction was first reached during Cycle 6a, and then in the other direction during Cycle 6b. When sliding occurred, the exterior tie-down rods were tightened to increase the available frictional resistance along the joint, and thereby increase the capacity of the wall.

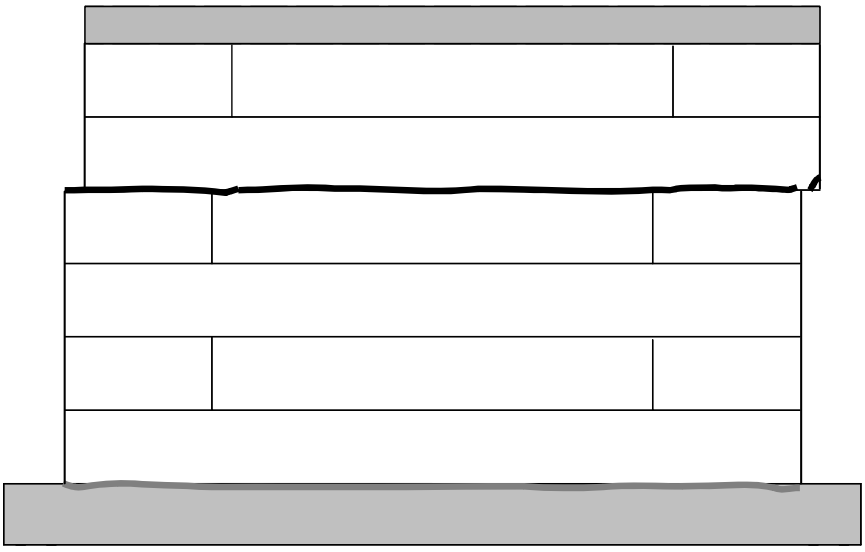

Figure 4-4: Cracking of Shear Wall Pilot Specimen 1 at Cycle 6a (horizontal crack at mortar joint under second panel from top)

1.2.3 Head-Joint Cracking

The next cracks, shown in Figure 4-5, formed during Cycles 7a and 7b, at the head joints between the 4 ft. (1.22 m) panels in the first and third courses from the top. These cracks formed because of insufficient bond in the head joints between panels. The small panels could rotate as discrete elements about their lower outside corners. The cracks on the north end of the wall opened during loading to the north and vice-versa for the south direction.

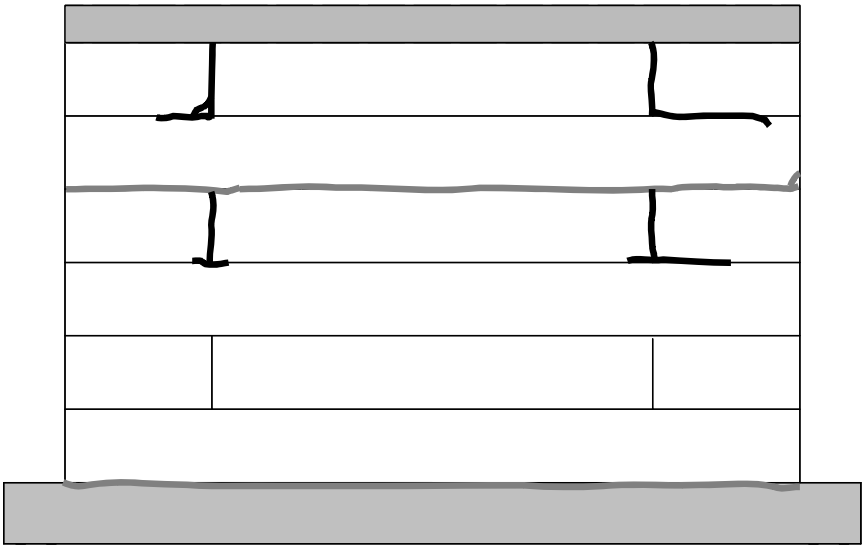

Figure 4-5: Cracking of Shear Wall Pilot Specimen 1 at Cycle 7 (vertical cracks along head joints)

Cycles 7b through 10a produced more cracks along all bed joints. The head joints bounding the short 4 ft. (1.22 m) blocks in the bottom course also opened. Local cracking occurred underneath those blocks as they rotated independently. This rotation also produced tensile splitting cracks. Figure 4-6 shows the wall after Cycle 10a.

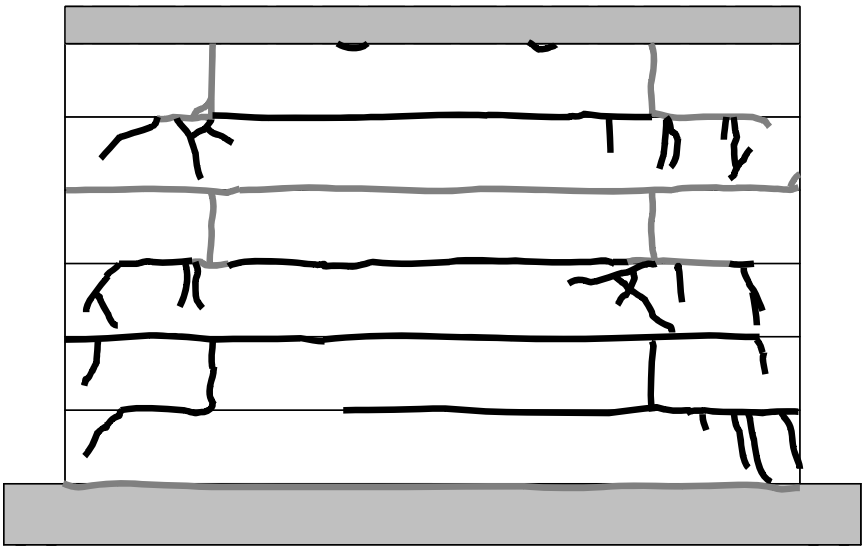

Figure 4-6: Cracking of Shear Wall Pilot Specimen 1 at Cycle 10a (more cracks in bed joints and head joints, plus local effects)

1.2.4 Diagonal Cracking

Finally, a compression strut formed in the bottom south corner of the wall. During Cycle 11a, the existing cracks continued to propagate. In Cycle 12a, the specimen failed in diagonal compression in the AAC panel in the bottom south corner. The final cracking pattern of Shear Wall Pilot Specimen 1 is shown in Figure 4-7.

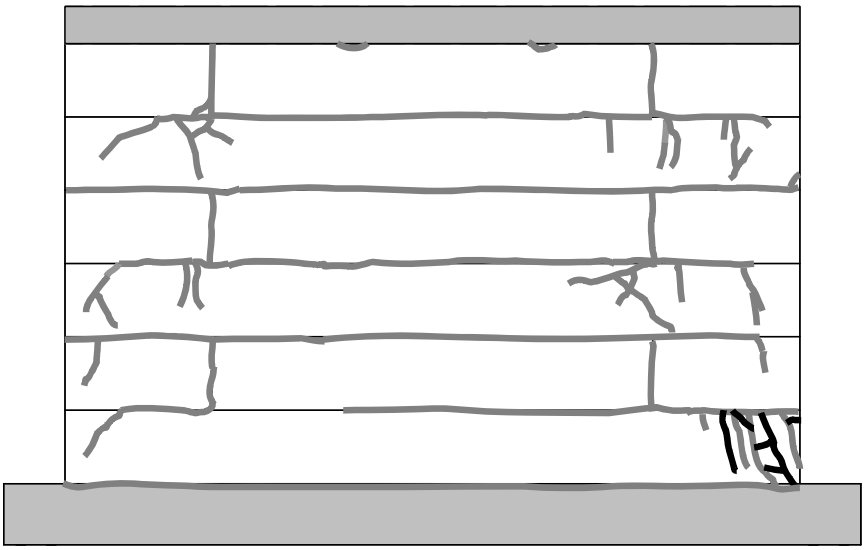

Figure 4-7: Cracking of Shear Wall Pilot Specimen 1 at end of test (crushing of AAC in lower south corner)

1.3 LOAD-DISPLACEMENT BEHAVIOR

In this section, load-displacement curves show applied in-plane shear versus lateral drift ratio, expressed as a percentage. As discussed in the previous section and shown in Figure 4-4, bed-joint cracking led to sliding between panels. This sliding is reflected in the load-displacement curves. To reduce the influence of this sliding, the threaded tie-down rods were tightened during the test. Points at which the tie-down force was increased are noted in this discussion.

The hysteretic load-displacement response of Shear Wall Pilot Specimen 1 is described in terms of "major events." These refer to points during the test when either the condition of the specimen changed (for example, flexural cracking or

head-joint cracking), or the external tie-down force was increased. Table 4-3 lists the major events and the load point at which they occurred.

Table 4-3: Description of Major Events for Shear Wall Pilot Specimen 1

Major Event	Load Point	Physical Description
1	57	Flexural crack at base
2	125	Large noise, crack formed at north buttress
3	146	Large noise at south end of specimen
4	154	Tightening of threaded rods
5	180	Additional tightening of threaded rods

The following list further describes the significance of the major events:

- At Major Event 1, a flexural crack formed at the base of the wall.
- At Major Event 2, a loud noise came from the north side of the wall, and vertical cracks formed between the hydrostone and the buttresses.
- At Major Event 3, a loud noise came from the south side of the wall (most likely from the wall slipping along the buttress on the south side) while loading to the south.
- At Major Event 4, the threaded rods were tightened after bed-joint slip.
- At Major Event 5, the threaded rods were tightened more.

1.3.1 Major Events 1 through 3

The hysteresis curve from the beginning of the test up to Major Event 2 is shown in Figure 4-8. Major Event 1 (flexural cracking) occurred at an applied

load of 6.5 kips (29.0 kN) and a drift ratio of 0.01%. The initial tangent stiffness K_o, also shown in Figure 4-8, is 550 kips/in. (101 kN/mm). The backbone stiffness, K_1, after Major Event 1 but prior to Major Event 2, is 365 kips/in. (63.9 kN/mm). In other words, initial flexural cracking reduced the specimen's lateral stiffness to about 65% of the initial stiffness.

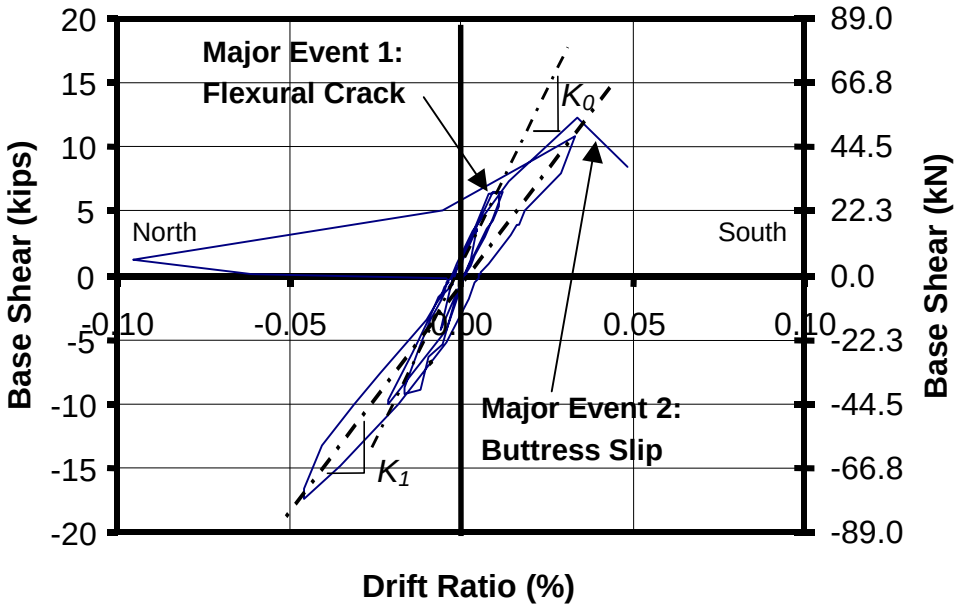

Figure 4-8: Base shear versus percent drift through Major Event 2

Prior to Major Event 2, an anomaly in the hysteresis loop can be seen, when the drift ratio suddenly increases to a value of –0.10%. This peak was not in the top of the wall displacement data but instead was introduced when base sliding was subtracted out. It is believed that the potentiometer that measures this

base slip was bumped or had some other sort of temporary anomaly, because the drift ratio soon returned to a consistent value.

Major Event 2 (buttress cracking) occurred at an applied load of 12.3 kips (54.7 kN) and a drift ratio of 0.03%. Major Event 3 (noise at south end) occurred at an applied load of -14.4 kips (-64.1 kN) and a drift ratio of 0.04%. As shown in Figures 4-8 and 4-9, the load-displacement curve drops abruptly at that point.

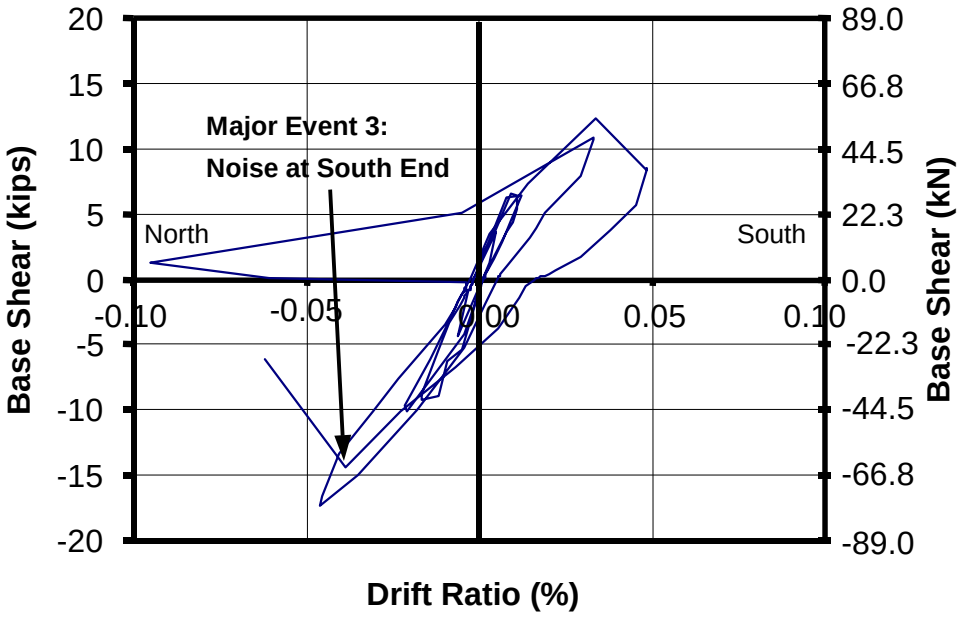

Figure 4-9: Base shear versus percent drift ratio through Major Event 3

1.3.2 Major Events 4 and 5

After the wall reached its capacity in the northward direction at Major Event 3 the specimen was unloaded, and had a permanent drift ratio of 0.06%.

Major Event 4 occurred when the threaded rods were tightened at this point. The force applied to the rods ranged between 3.5 kips (15.6 kN) and 5 kips (22.2 kN).

As shown in Figure 4-10, after the rods were tightened, loading was applied to the south, and was increased to 12.9 kips (57.6 kN). At this load sliding began along bed joints, and continued until the test was paused at a drift ratio of 0.20% and the specimen was unloaded. At this point the threaded rods were tightened for the second time (Major Event 5).

The tie-down force was increased to 30 kips (133.4 kN) on the north end and about half that value on the south end. The tie-down force at the south end of the specimen is not known precisely, because the innermost force washer at that end did not read properly during the test. The washers were checked after the test and found to be working as expected, so the improper readings were probably due to incorrect wiring. The force washer on the outermost rod at the south end indicated a tie-down force of 11 kips (48.9 kN). The increased tie-down force induced in Major Event 4 provided sufficient tie-down force so that the subsequent behavior of the specimen was still probably governed by bed-joint sliding, but at a higher capacity than would otherwise have been the case.

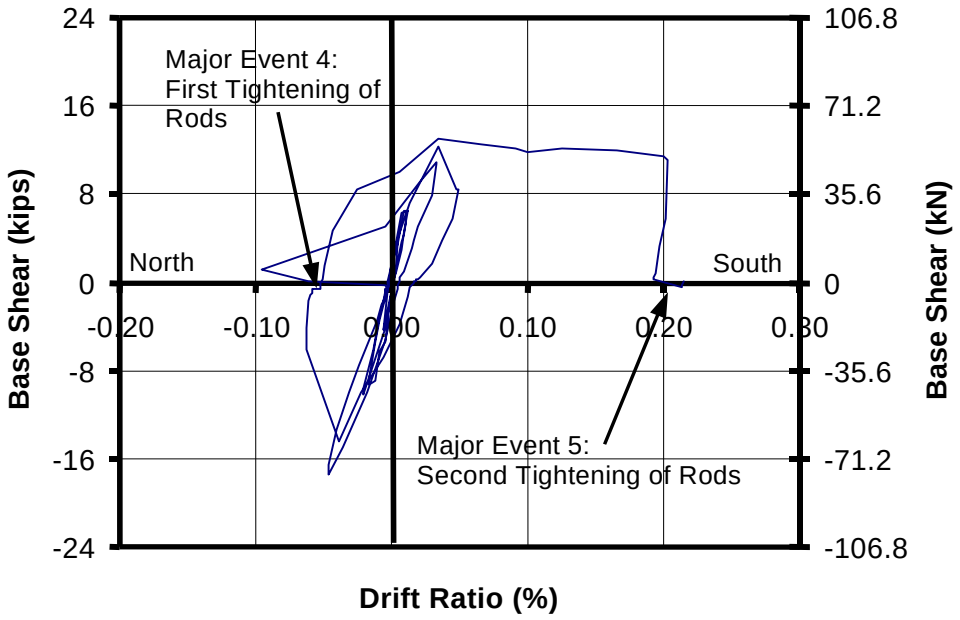

Figure 4-10: Base shear versus percent drift ratio through Major Event 5

1.3.3 Behavior After Major Event 5

After Major Event 5, the load was again applied in the south direction. The subsequent load-displacement curve is shown in Figure 4-11. The increased tie-down force induced in Major Event 5 resulted in an increased capacity after that point. The wall had a peak applied load of 21.1 kips (93.7 kN) in the south (positive) direction and 21.4 kips (95.2 kN) in the north (negative) direction.

When the specimen was loaded in the south direction during Cycle 8a, the dips in the load-displacement curve represent pauses in loading to mark cracks that were forming in the panels (Figure 4-6). Some cracks were inclined at approximately 45 degrees (typical of diagonal tension cracks); others were more

vertical due to local orientations of principal tensile stresses and local movement of individual panels.

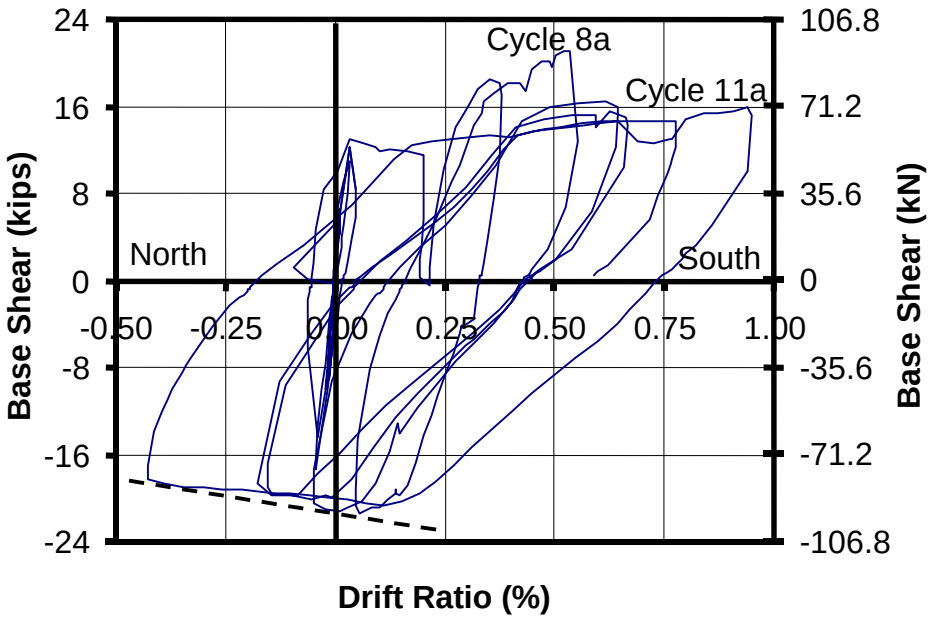

Figure 4-11: Base shear versus percent drift ratio after Major Event 5

After Cycle 8a, the wall's backbone stiffness decreased from roughly 88 kips/in. (15.5 kN/mm) to about 44 kips/in. (7.7 kN/mm). The lateral capacity decreased from about 21 kips (93 kN) to about 16 kips (71 kN) in the south direction. In the north direction, however, the load did not drop off abruptly as it had to the south. Instead, it slowly decreased with increasing drift, as shown by the dashed line in Figure 4-11. The clamping force on the north side of the wall was significantly higher than on the south side of the wall; this could have caused a decrease in capacity at larger displacements due to P-Δ effects.

During Cycle 11a the applied load decreased from 14.7 kips (65.4 kN) to 12.7 kips (56.5 kN) and at Load Point 427 a large crack formed at the compression toe on the south end of the wall (Figure 4-12). This crack indicated the imminent failure of the diagonal compression strut at the base of the wall, due to a combination of diagonal compression and shear. Prior to complete failure of the specimen, however, the load was reversed (Cycle 11b) since the predetermined displacement had been reached. As the specimen was loaded to the north, the cracks that had formed in the south toe had no apparent effect on the behavior of the wall, which reached its predetermined displacement for Cycle 11b without compression failure of the north toe.

Finally, as the applied load increased to the south during Cycle 12a, the compression strut exhibited gross cracking and spalling of the AAC cover at the south toe (Figure 4-12). The inclined cracking also separated the compression toe of the wall into separate, smaller inclined struts, whose diminished cross-sectional area made them susceptible to buckling as well as material failure. Figure 4-13 shows this compression toe failure from the back of the wall.

Figure 4-12: Cracks and spalled concrete at south end of Shear Wall Pilot Specimen 1 at end of test

Figure 4-13: Back face of compression toe at end of test, Shear Wall Pilot Specimen 1

The condition of the wall at the end of the test is shown in Figure 4-14. Cracks were concentrated at the north end of the specimen when load was applied to the north, and at the south end when load was applied to the south. At the end of the test, the wall had been reduced to a set of compression struts. The stiffness and strength of the compression struts were strongly influenced by the opening of head joints (Figure 4-15) and the sliding across bed joints.

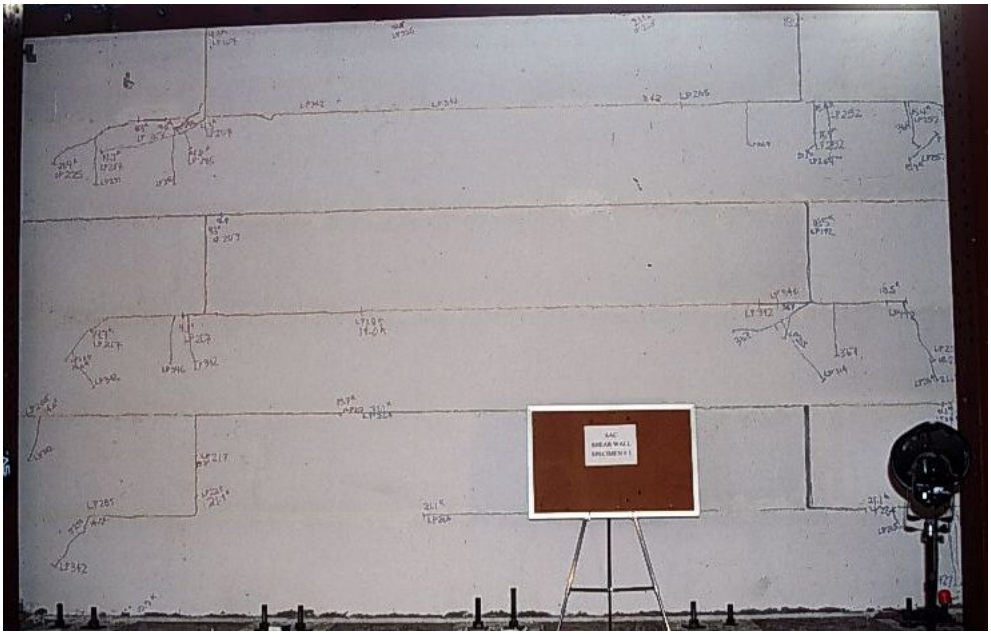

Figure 4-14: Shear Wall Pilot Specimen 1 at end of test

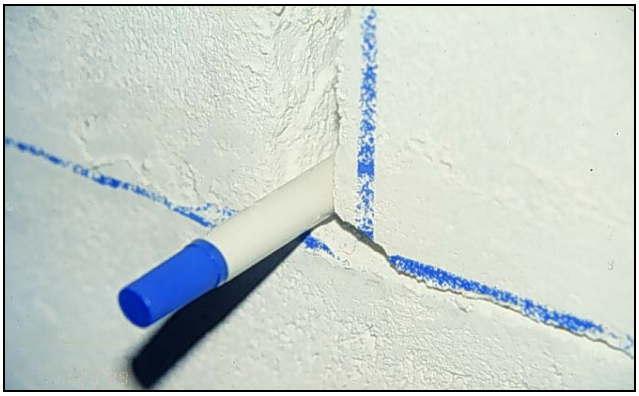

Figure 4-15: Openings of head and bed joints at the end of the test, Shear Wall Pilot Specimen 1

CHAPTER 1: RESULTS FROM TEST ON SHEAR WALL PILOT SPECIMEN 2

This chapter presents the results and behavior from the test on Shear Wall Pilot Specimen 2. In this section, the response of Shear Wall Pilot Specimen 2 is discussed, first with respect to load history, then with respect to the observed behavior and cracking patterns, and finally with respect to recorded load-displacement behavior. A complete list of the data collected during this test is presented in Section 3.4. Only the data necessary to describe the above results are presented here.

As mentioned in the previous chapter, re-calibration of the load cells showed that they were under-reporting the load by about 4%. For these tests, the 4% error results in the maximum load being under-reported by about 1 kip (4.5 kN). Therefore, the data from this test were not modified to include the 4% increase.

1.1 LOADING HISTORY

The planned loading history for Shear Wall Pilot Specimen 2 is shown in Figure 3-6. As described in Chapter 3, the amplitudes of each cycle were established by predicted major events. The predetermined load values for this specimen, which are higher than for Pilot Specimen 1 because of the initial 20 kips (89 kN) of axial load, are shown in Table 5-1.

Table 5-1: Predetermined load values for Shear Wall Pilot Specimen 2

Predetermined Value (PV)	Major Event	Predicted Load
1	flexural cracking	27.7 kips (123 kN)
2	web shear cracking	61.3 kips (273 kN)
3	yielding of external flexural steel	197 kips (603 kN)

Table 5-2, Figure 5-1, and Figure 5-2 break the data into cycles, which are identified by the numbers at the top of Figure 5-1 and Figure 5-2. Each cycle contains a number of load points at which data was recorded. For reference throughout this thesis, Table 5-2 shows which load points occurred during each cycle. The load points are identified by numbers that increase monotonically throughout the test. Loading to the south is considered to be positive, and is designated by an "a" next to the cycle number. Loading to the north is considered to be negative, and is designated by a "b" next to the cycle number.

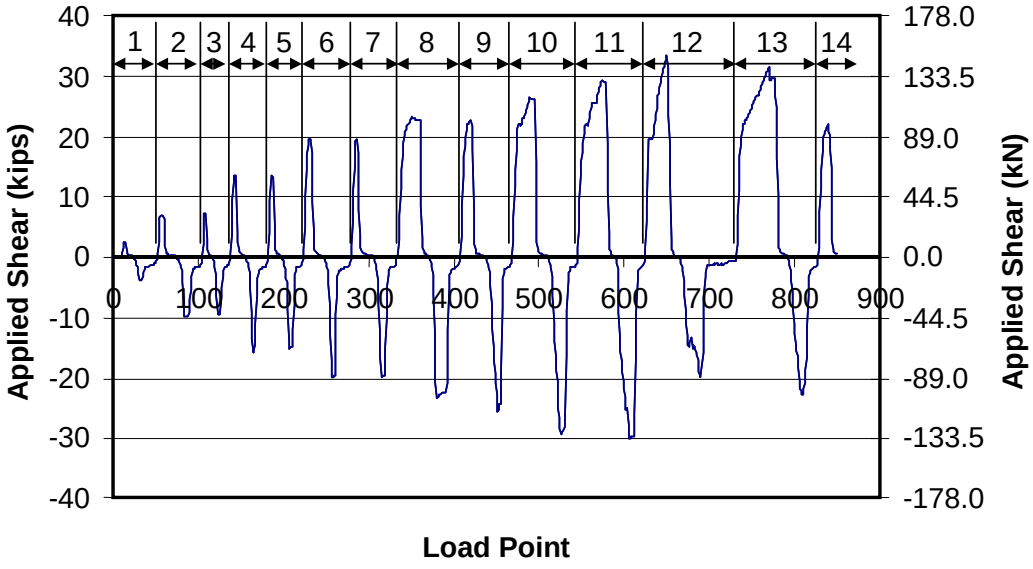

Figure 5-1: Actual loading history for Shear Wall Pilot Specimen 2 (numbers at top of plot designate cycle numbers)

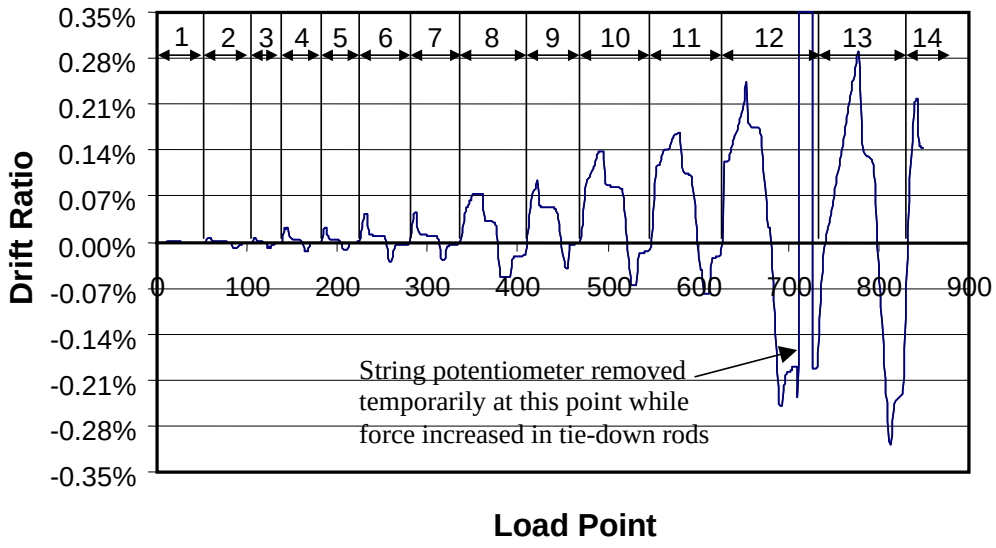

Figure 5-2: Actual displacement history for Shear Wall Pilot Specimen 2 (numbers at top of plot designate cycle numbers)

Table 5-2: Maximum load and drift ratio in each cycle for Shear Wall Pilot Specimen 2

Cycle	Load Points	Maximum Applied Load kips (kN)	Maximum Drift Ratio
1a	1 – 24	2.3 (10.1)	0.001%
1b	25 – 52	-4.0 (-17.6)	-0.003%
2a	53 – 75	6.9 (30.8)	0.007%
2b	76 – 105	-9.8 (-43.4)	-0.008%
3a	106 – 116	7.0 (31.3)	0.007%
3b	117 – 137	-9.6 (-42.6)	-0.008%
4a	138 – 155	13.7 (60.8)	0.021%
4b	156 – 181	-15.8 (-70.3)	-0.014%
5a	182 – 197	13.5 (60.1)	0.022%
5b	198 – 223	-15.0 (-66.7)	-0.013%
6a	224 – 246	19.5 (86.9)	0.043%
6b	247 – 279	-20.0 (-88.8)	-0.029%
7a	280 – 305	19.6 (87.0)	0.045%
7b	306 – 333	-19.7 (-87.8)	-0.028%
8a	334 – 370	23.3 (103.5)	0.075%
8b	371 – 407	-23.3 (103.8)	-0.052%
9a	408 – 436	22.9 (101.9)	0.095%
9b	437 – 467	-25.7 (-114.5)	-0.039%
10a	468 – 509	26.3 (116.9)	0.137%
10b	510 – 545	-29.3 (-130.3)	-0.066%
11a	546 – 588	29.4 (130.7)	0.166%
11b	589 – 624	-30.0 (-133.3)	-0.079%
12a	625 – 664	33.5 (149.0)	0.245%
12b	665 – 730	-19.8 (-88.3)	-0.249%
13a	731 – 791	31.4 (140.0)	0.290%
13b	792 – 827	-22.9 (-101.7)	-0.308%
14a	828 – 849	22.0 (97.6)	0.218%

Like Shear Wall Pilot Specimen 1, the amplitude of the cycles was initially controlled by predetermined force levels. The first cycle of about 3 kips

(13.3 kN) was to check that the data acquisition system was giving reasonable results prior to proceeding with the test. The first predetermined target value was 22 kips (97.9 kN) which corresponded to the predicted flexural cracking capacity. This value was divided into thirds, and sets of two full cycles (Cycles 2-7) were applied to force levels of about 7, 15, and 22 kips (31.1, 66.7, and 97.9 kN respectively). The peak load and drift ratio values are shown in Table 5-2.

The next major event was web shear cracking, predicted at 55 kips (244.7 kN). The difference between this value and the previous target value of 22 kips (97.9 kN) was divided into thirds. When loading to reach the next incremental load step of 33 kips (146.8 kN), the wall began to slide along the base. As mentioned earlier and discussed more thoroughly later in this thesis, thin plates were inserted between the wall and the buttresses to prevent this sliding. Cycles 8 through 12 were used to try to reach the load of 33 kips (146.8 kN), while inserting plates to stop the sliding.

Between Cycles 12 and 13, the post-tensioning force in the tie-down rods was increased from the initial 20 kips (89.0 kips) to about 55 kips (244.7 kN) to try to prevent slip along cracks that had formed along the top of the wall. These cracks and their implications are discussed later in this thesis. The point at which the rods were tightened is shown in Figure 5-2. Also, during this increase in tie-down force, the wire to the horizontal displacement potentiometer was removed, which resulted in a large spurious displacement to the south. Prior to resuming the test, the potentiometer was re-attached and the displacement corrected to its value prior to removal.

During Cycle 13, inspection of the relation between base shear and in-plane drift showed that applied load was approaching the in-plane capacity of the wall. At this point, the loading cycles were changed from force- to displacement-controlled. For Cycle 13, a drift limit of about 0.27% was imposed. One full cycle was completed to this limit. While being loaded to that drift limit again during Cycle 14a, the wall lost significant capacity compared to the previous cycle, and compression struts formed at the ends of the wall. Therefore, the test was stopped at a drift ratio of about 0.20% and a force level of 22 kips (97.8 kN).

1.2 SEQUENCE OF CRACK FORMATION

1.2.1 Flexural Cracking at Base

As in Shear Wall Pilot Specimen 1, prior to testing, shrinkage cracks had already formed along the base of the wall through the mortar joint (Figure 5-3). These cracks were the first to open during the test, and appeared as flexural cracks in the tension side of the wall during Cycles 6a and 6b.

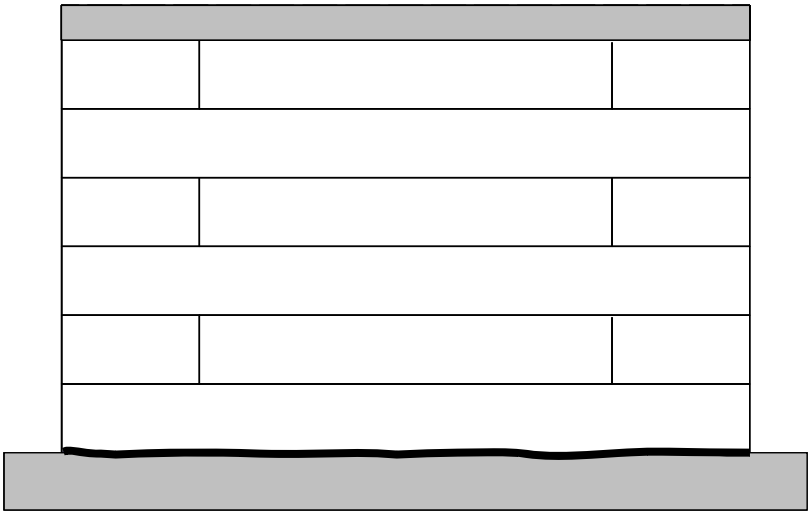

Figure 5-3: Initial shrinkage crack at base of Shear Wall Pilot Specimen 2

1.2.2 Local Cracking at Patches

The next cracks to form were local cracks around patching between the 4 ft. (1.22 m) panel at the south end, and the 12 ft. (3.66 m) panels in the second row from the bottom (Figure 5-4). In that and the following figures, black lines represent new cracks and gray lines represent previously described cracks. The patches were placed during construction to repair points where the panels had been damaged during shipping and installation. The patching mortar was supplied by Ytong Florida, Ltd. (Haines City, Florida) and was applied to the wall using a trowel. The cracks were cosmetic only, and did not appear to affect stiffness or strength.

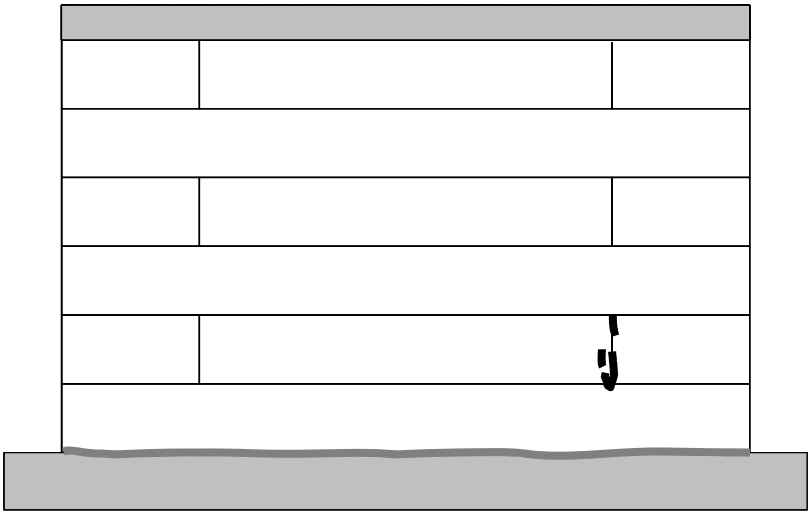

Figure 5-4: Cracking of Shear Wall Pilot Specimen 2 during Cycle 11b (local cracking at patch)

1.2.3 Flexural Crack at Center of Panel

The next crack, shown in Figure 5-5, formed at the head joints between the northernmost 4 ft. (1.22 m) panel and the center 12 ft. (16.27 m) panel in the top row during loading to the south. The crack started in the head joint, most likely due to poor bond between the two panels. The crack appeared to propagate from a crack that had been caused by the post-tensioned rods that clamp the channels to the specimen. After the vertical crack formed, the center panels began to act independently, and the diagonal crack formed due to local tensile stresses.

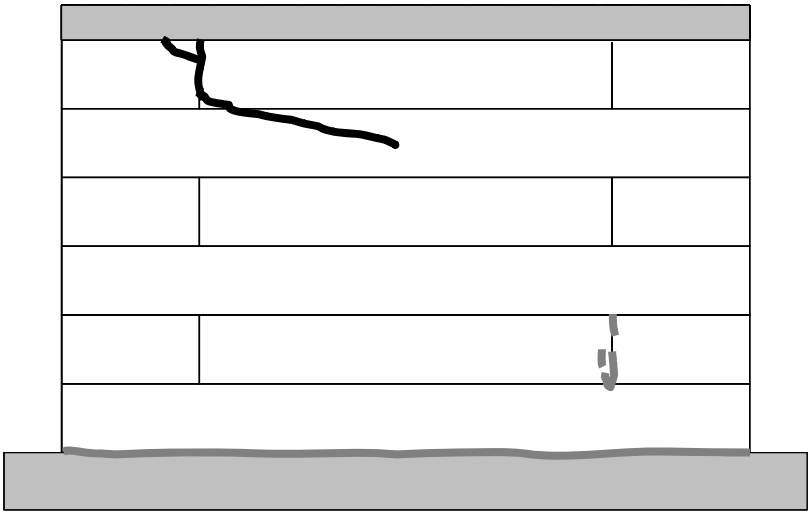

Figure 5-5: Cracking of Shear Wall Pilot Specimen 2 at Cycle 12a (head-joint shear cracking in top course)

1.2.4 Horizontal Tensile Bond Beam Crack

After the loading had been stopped and while the previous head-joint shear cracks were being marked, a crack formed at the center of the wall just underneath the bond beam due to tensile forces at the center of the wall from the flexural deformation of the channels, which were not originally designed to carry vertical loads. When a force of 20 kips (89.0 kN) was put into the tie-down rods, compression, denoted by "C" in Figure 5-6, was introduced into the ends of the wall. The resulting channel deformations led to an uplift force, shown by "T" in Figure 5-6, in the center of the wall. When the head-joint crack formed, the load path at the top of the wall changed enough to allow the splitting crack to form (Figure 5-7).

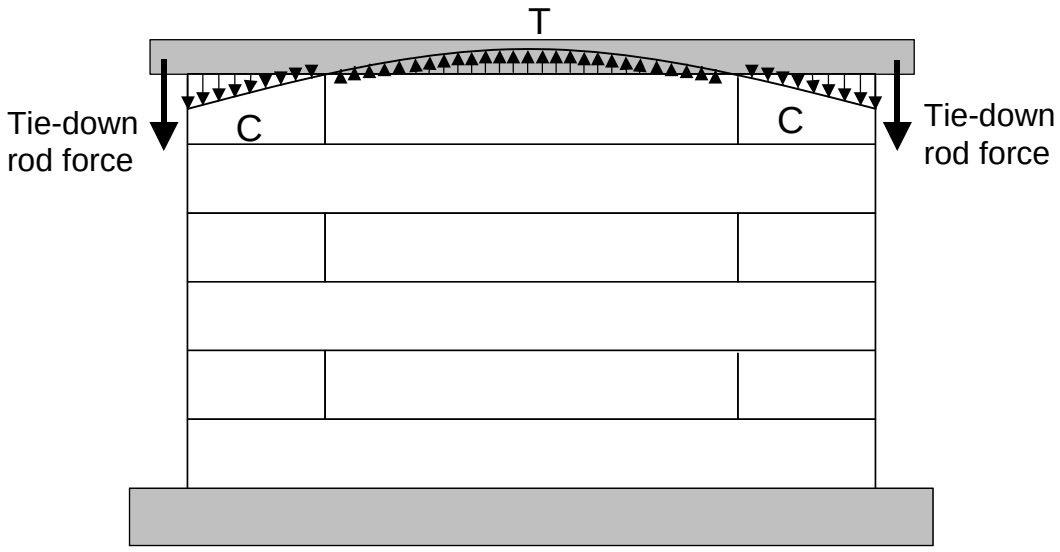

Figure 5-6: Elastic stress distribution at top of wall from flexural deformations of bond beam

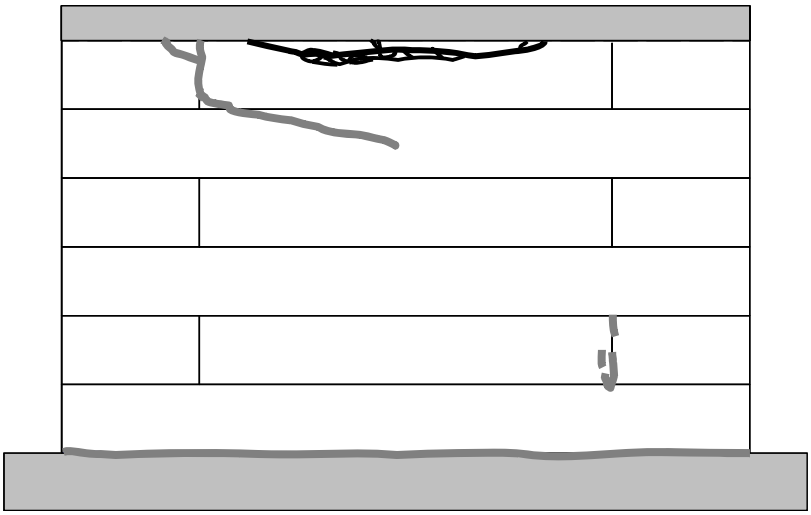

Figure 5-7: Cracking of specimen at Cycle 12a (tensile bond beam crack)

1.2.5 Discrete Block Rotation

After the horizontal crack formed below the bond beam, the beam moved upwards in the middle of the wall resulting in very little contact between it and the wall. Most of the applied horizontal load had to be transferred over the compressive regions at the ends of the loading beam (Figure 5-8).

When the tensile bond beam crack formed, the entire applied shear was transferred to the end panels. Loading was to the south. The transfer of load caused the 4 ft. (1.22 m) panels to act like individual elements. The head joints of these panels failed due to a lack of bond (see below). This allowed the panels to rotate independently, and immediately caused the flexural cracks shown in Figure 5-11. The independent panel behavior is similar to that which occurred during Pilot Test 1. When the load was reversed and applied in the north direction in Cycle 12b, the north end panel rotated about its outside bottom corner, producing the flexural crack around the panel at the north end.

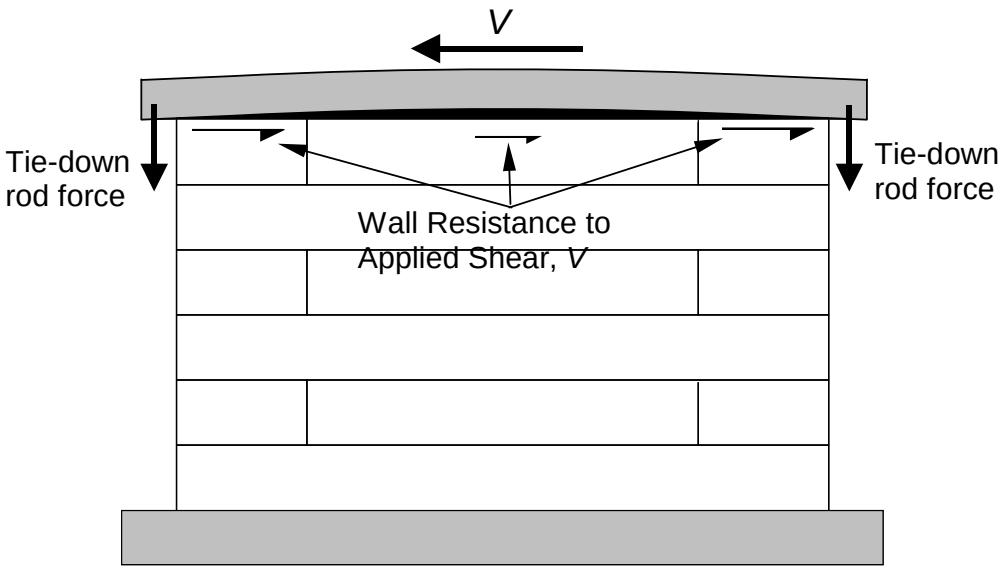

Figure 5-8: Wall resistance to applied shear after bending of bond beam

Because the shear force was resisted primarily at the ends of the wall, and because of the weak bond in the head joints between panels (Figure 5-9), the 4 ft. (1.22 m) panels acted independently (Figure 5-10).

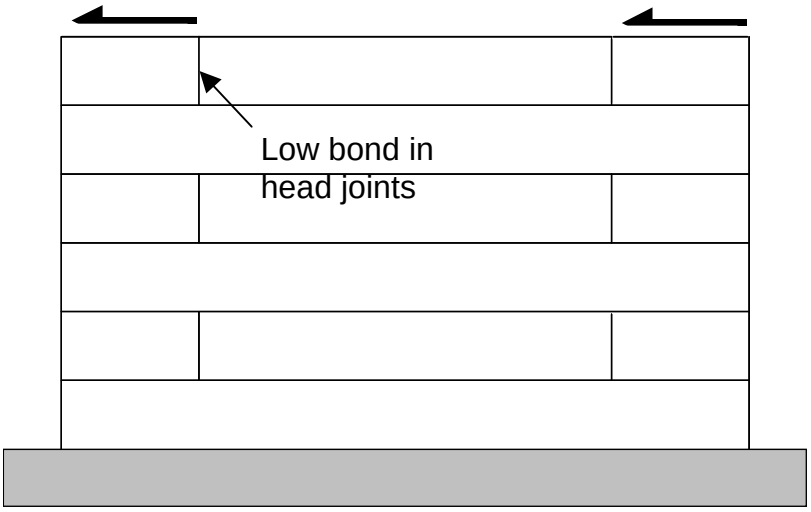

Figure 5-9: Shear force transferred to top of the wall

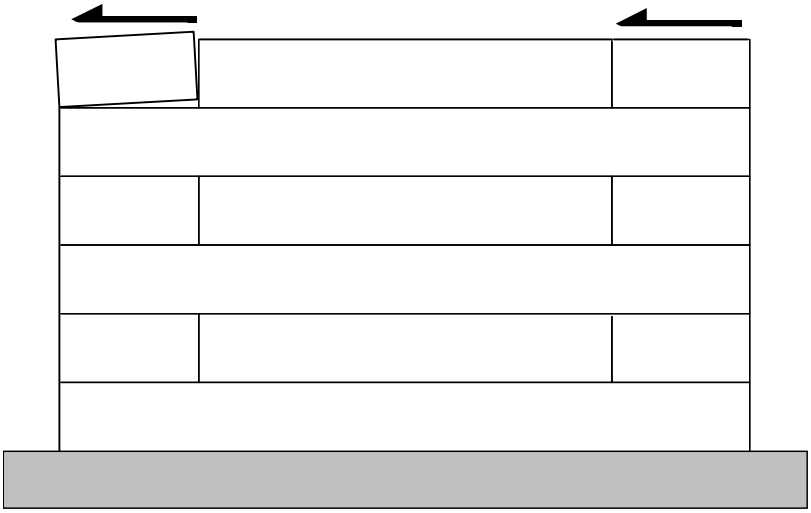

Figure 5-10: Flexural rotation of individual panel element

This individual flexural response led to flexural cracks in the bed joint below the rotating end panels (Figure 5-11). Figure 5-11 also shows tension cracks in the panels below the rotating panels that formed when flexural cracks propagated along the base of the rotating panels and then turned downward.

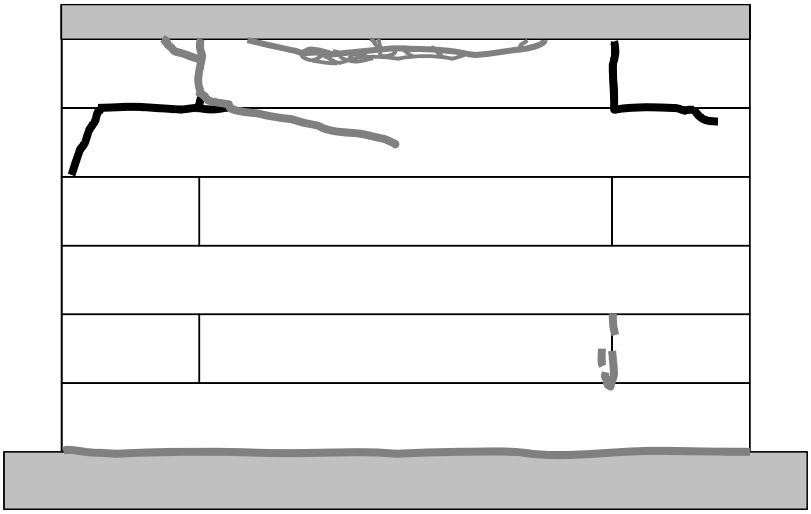

Figure 5-11: Cracking of Shear Wall Pilot Specimen 2 at Cycle 12 (discrete block rotation)

1.2.6 Local Diagonal Splitting Cracks

After the above-mentioned cracks had formed, the wall appeared to be sliding back and forth; the force in the tie-down rods was therefore increased from 5 kips (22.2 kN) per rod (a total of 20 kips, or 89.0 kN) to 14 kips (62.3 kN) per rod (a total of 56 kips, or (249.1 kN). As the rods were tightened, the hogging

deformation of the beam increased, the horizontal cracks at the middle of the wall widened, and the ends of the wall showed signs of crushing.

After the tie-down force was increased and the load cycles were continued, more evidence appeared supporting the above hypothesis. The flexural cracks in the bed joints under the end panels propagated into the panels below each as each end block rotated about its exterior toe (Figure 5-12). Also, the head joints opened and closed corresponding to the direction of load.

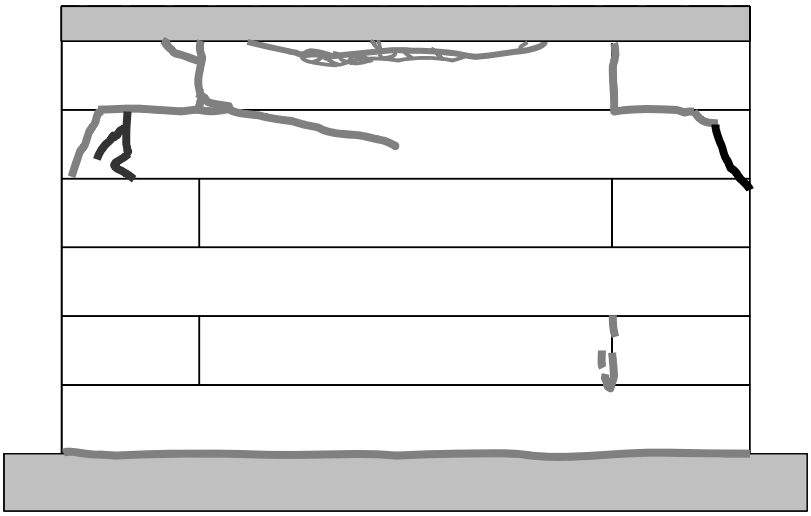

Figure 5-12: Cracking of Shear Wall Pilot Specimen 2 at Cycle 13 (local diagonal splitting cracks)

1.2.7 Crushing at End of the Wall

During Cycles 13b and 14a, the AAC at the ends of the wall underneath the exterior top panels began to spall, as shown by the hatched area in Figure 5-13. Finally, a compression strut formed at the south end during Cycle 14a,

underneath the rotating panel. At this point, it was determined that the wall had reached its capacity, and that it would be unsafe to continue loading. The wall was unloaded and the test was ended.

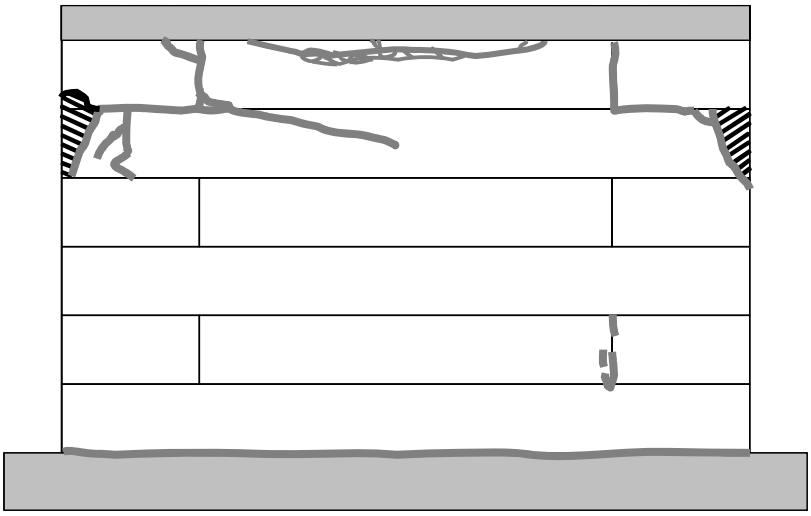

Figure 5-13: Cracking of Shear Wall Pilot Specimen 2 at Cycles 14a (spalling and crushing at ends of wall)

1.3 LOAD-DISPLACEMENT BEHAVIOR

In this section, load-displacement curves show applied in-plane shear versus the lateral drift ratio, expressed as a percentage. The lateral drift ratio is the specimen's in-plane horizontal displacement at the level of load application, divided by its height (the distance between the top of the base and the level of load application).

The horizontal displacement shown in the curves below was adjusted for sliding at the base of the wall. To correct for the sliding, the slip between the wall and the base was subtracted from the total displacement measured at the top of the wall. The goal of this correction was to isolate the behavior of the wall itself, so that an accurate drift ratio could be calculated. In an actual building and in future tests sliding will be prevented through methods discussed later in this thesis.

The hysteretic load-displacement response of Shear Wall Pilot Specimen 2 is described in terms of "major events." Major events refer to points during the test when either the condition of the specimen changed (for example, flexural cracking or head-joint cracking), or the external tie-down force was increased. Table 5-3 lists the major events and the load point at which they occurred.

As discussed in the previous section, a horizontal crack just below the loading beam led to rocking of the end panels and sliding of the bond beam above the center panel. Prior to determining the cause of the horizontal crack at the top of the wall the tie-down rods were tightened in an attempt to reduce sliding at the top of the wall. The point at which the rods were tightened is noted in this discussion.

Table 5-3: Description of Major Events for Shear Wall Pilot Specimen 2

Major Event	Load Point	Physical Description
1	231	flexural crack at base
2	652	discrete block rotation and tensile bond beam crack
3	696	tightening of threaded rods

The following list further describes the significance of the major events:

- Major Event 1 was the formation of a flexural crack at the base of the wall.
- Major Event 2 was the formation of a large splitting crack just below the bond beam and the development of local flexural cracks as the panels in the top row acted as discrete elements.
- Major Event 3 was when the threaded rods were tightened to try to resist sliding shear that was originally thought to be the cause of the low lateral stiffness of the wall.

1.3.1 Major Event 1

The hysteresis curve from the beginning of the test up to Major Event 1 is shown in Figure 5-14. Major Event 1 (flexural cracking) occurred at an applied load of 19.5 kips (86.5 kN) and a drift ratio of 0.01%. This load is much higher than the load that caused flexural cracking in Shear Wall Pilot Specimen 1 -- 6.3 kips (28.0 kN). The predicted load to cause shear cracking was 22.3 kips (99.2 kN). The results of Shear Wall Pilot Specimen 2 more closely match the results of the predicted value than do those of Shear Wall Pilot Specimen 1. The increased flexural capacity of Specimen 2 is most likely due to the increased axial force on the wall. The flexural cracking capacity of the walls probably did not reach the predicted value because of the initial shrinkage crack. The initial tangent stiffness K_o, also shown in Figure 5-14, is 689 kips/in. (120.7 kN/mm).

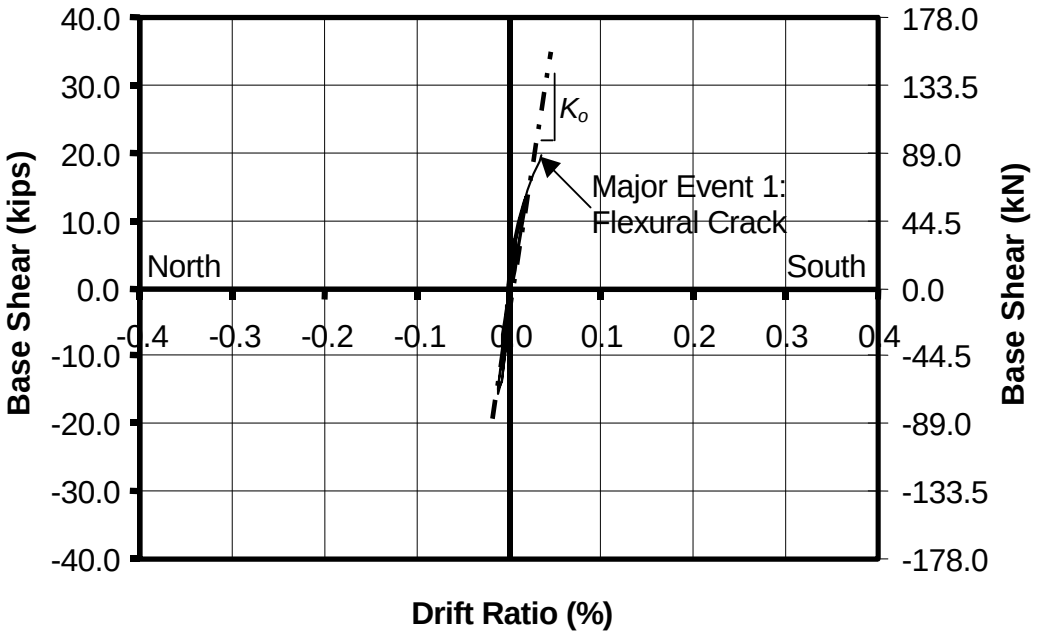

Figure 5-14: Load displacement curve through Major Event 1

1.3.2 Major Event 2

After flexural cracking occurred, the overall stiffness of the wall decreased. This is shown in Figure 5-15, which shows the backbone stiffness, K_1, of the response after Major Event 1 but prior to Major Event 2. The backbone stiffness, K_1, is 326.4 kips/in. (57.2 kN/mm). In other words, initial flexural cracking reduced the specimen's lateral stiffness to about 50% of its initial value.

When the first individual panel flexural crack formed, the predetermined value of 33 kips (146.8 kN) had been reached. When the crack occurred, the applied load was 33.5 kips (149.0 kN), and was just about to be reversed. At this point the drift ratio was 0.10%. When the load was stopped and cracks were

being marked on the wall, the horizontal tension crack formed just below the bond beam. This also led to the formation of another flexural crack at the bed joint of the southernmost panel in the top course. This series of cracks led to the sudden decrease in the applied load (23.6 kips, or 104.8 kN), and to a sudden increase in the drift ratio, to 0.12% (Figure 5-15).

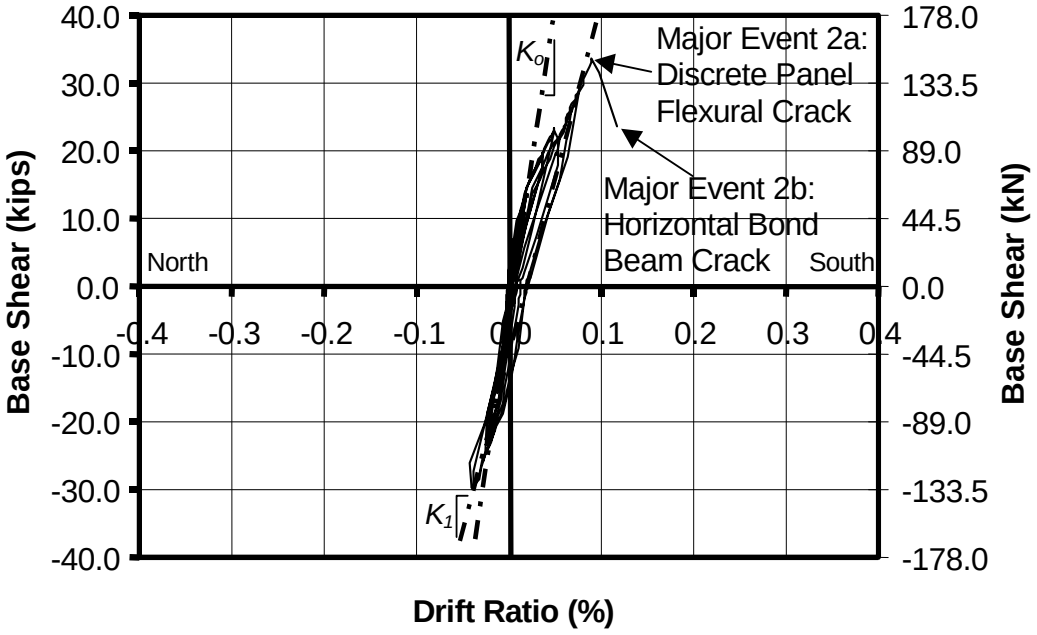

Figure 5-15: Load-displacement curve through Major Event 1

1.3.3 Behavior After Major Event 2

Since the predetermined value of 33 kips (146.8 kN) had been reached, the load was then cycled in the reverse direction. As the load increased to the north, the load-carrying capacity of the wall leveled off at around 20 kips (89.0 kN),

accompanied by significant deformation (Figure 5-16). Since sliding was believed to be the cause of the displacement, the tie-down rods were tightened to increase the sliding shear capacity in an attempt to reach the web shear capacity of the wall. This point is shown in Figure 5-16.

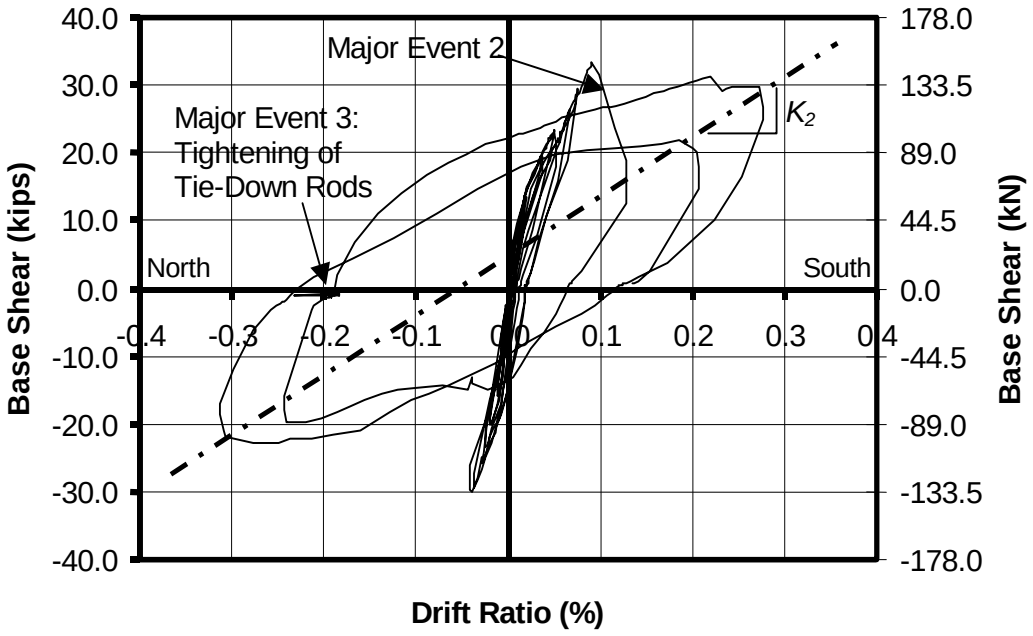

Figure 5-16: Load displacement curve through the end of the test

In evaluating the behavior of Pilot Specimen 2 after the test, it was realized that increasing the tie-down force might have actually made the problem worse because it hogged the bond beam so that only its ends were in contact with the wall. Therefore, only the 4 ft (1.22 m) end panels resisted the applied lateral force. As Figure 5-16 shows, the lateral behavior did not change significantly after the tie-down force was increased. During these loops, loading was

controlled by displacement. The next cycle had a maximum drift ratio of about 0.3%. The backbone stiffness, K_2, during this part of the test was about 60 kips/in. (10.5 kN/mm), as shown in Figure 5-16. After only two more cycles, the AAC in the wall began to develop vertical splitting cracks which separated the 4 ft (1.22 m) panels into smaller vertical compression struts at the end of the wall panels. Figure 5-17 shows the compression struts that formed at the end of the wall and that occurred from the panels acting in flexure as discussed above in Sections 5.2.6 and 5.2.7.

Figure 5-17: Cracked and spalled AAC on back of south end of Shear Wall Pilot Specimen 2 at end of test

The decreased cross-sectional area and decreased stability of the compression struts made the end of the wall susceptible to material failure and buckling. Figure 5-18 shows the cracking and spalling at the south end of the wall at the end of the test.

Figure 5-18: Cracked and spalled AAC at south end of Shear Wall Pilot Specimen 2 at end of test

The gross cracking at the end of the wall and the loss in capacity suggested that failure was imminent, so the test was stopped. The photograph of

the final cracking pattern of Shear Wall Pilot Specimen 2 is shown in Figure 5-19; a drawing of it is shown in Figure 5-13. Most cracking was isolated to the top of the wall. The thin-bed mortar joints in Pilot Specimen 2 behaved much better than those of Pilot Specimen 1, even though the maximum load was about 50% higher. Mortar joints cracked only around the top two 4 ft (1.22 m) panels; in Shear Wall Pilot Specimen 1, in contrast, mortar-joint cracks were distributed throughout the wall.

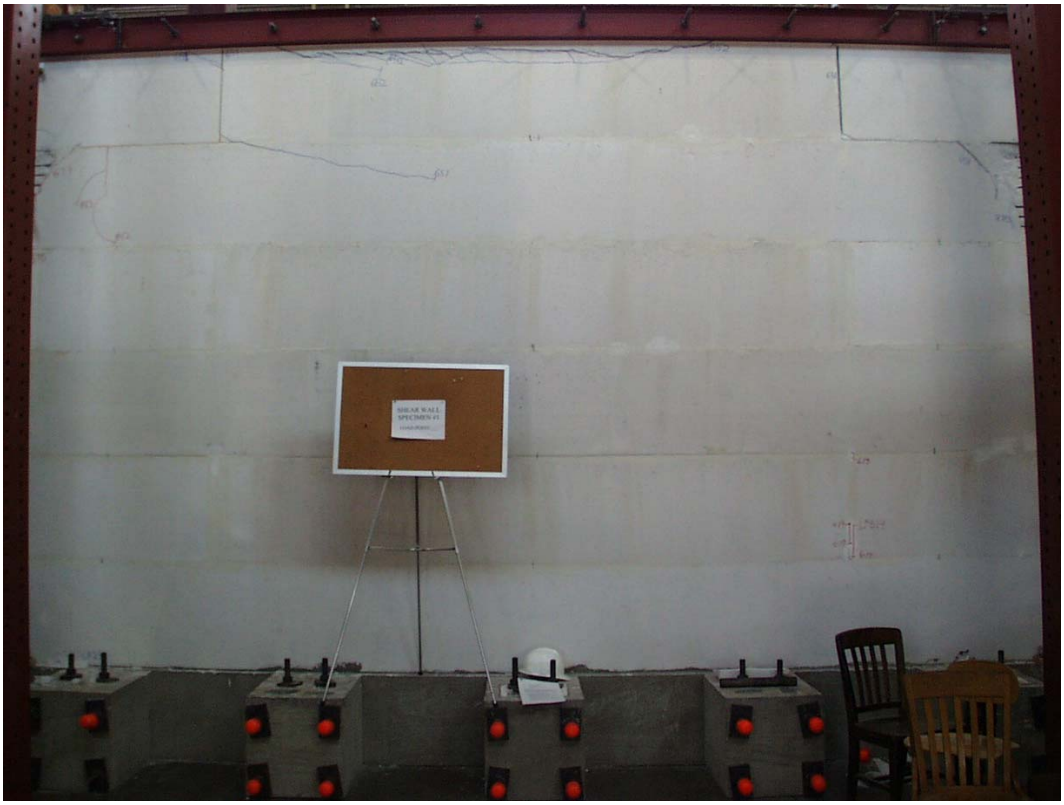

Figure 5-19: Shear Wall Pilot Specimen 2 at end of test

CHAPTER 1: SIGNIFICANCE OF RESULTS AND RECOMMENDATIONS

Under test, AACA Shear Wall Pilot Specimens 1 and 2 exhibited many kinds of behavior that had been anticipated and included in behavioral models used to predict their load-displacement behavior under reversed cyclic loading. Most significantly, enough load could not be applied to force web shear cracking without first producing other failure mechanisms. During the test of Shear Wall Pilot Specimen 1, sliding along mortar joints was observed, along with pinching at the bottom corners from the buttresses.

From the results of the first test, we were able to improve the construction and testing procedures prior to testing Shear Wall Pilot Specimen 2. During the test of Shear Wall Pilot Specimen 2 we again saw many kinds of behavior that had been anticipated and had been used to develop behavioral models. As in the first test, we saw behavior that deviated from that anticipated. Unlike the first test, behavior models for the entire wall were relatively accurate; local behavior, though, did not allow us to reach the goal of forcing web shear cracking.

The new observed behavior will be used to further refine the original models described in Chapter 2 and increase their probable value for predicting the behavior of subsequent specimens, and ultimately as design tools.

Some of the observed behavior not anticipated was:

- separation of panels along mortar joints;
- tensile cracking around the loading beam; and

- splitting and crushing of panels without yielding of the internal reinforcement.

Those are the topics of this section.

1.1 INTEGRITY OF THIN-BED MORTAR JOINTS

1.1.1 Integrity and Strength of Thin-Bed Mortar Joints of Shear Wall Pilot Specimen 1

The observation of joint failures requires a review of the integrity and strength of the thin-bed mortar. Shear Wall Pilot Specimen 1 was constructed using thin-bed mortar supplied by Contec Mexicana; was applied with a toothed trowel as directed by the Hebel instructional video (Hebel 1999b); and under construction supervision supplied by Contec. Bed joints between panels were formed using one layer of thin-bed mortar applied along the length of the lower panel. After the upper panel was placed on the mortar and set in place, light could be seen through the bed joints, indicating incomplete contact between the mortar and the panels. To mitigate this problem, mortar was applied to the sides of the bed-joint gaps, as directed by the construction supervisor. The problem was not as noticeable in the head joints. It is believed that the gaps in the head joints were filled in better because mortar was placed on both faces defining the joint.

After the test, when Shear Wall Pilot Specimen 1 was dismantled, a photograph of a typical bed joint between large panels (Figure 6-1) clearly shows that the thin-bed mortar contacted the overlying panel over at most 20% of the bed-joint area. The ridges visible in the photo are formed by the special spreading

trowel when the thin-bed mortar is applied. When a ridge remains, it implies insufficient bond on that part of the joint. The smooth areas, in contrast, are locations of full contact. Possible reasons for this low extent of bond are:

- the mortar joint was not thick enough to compensate for the dimensional tolerances of the large panels along the bed joints; or
- during construction, the thin-bed mortar had begun to set before the overlying panel was placed on top of it.

Figure 6-1: Typical thin-bed joint in Shear Wall Pilot Specimen 1

Examination of the dismantled Shear Wall Pilot Specimen 1 revealed a greater extent of bond in the head joints (from 30% to 70%) (Figure 6-2). This

difference is attributed to the fact that the head joints were thicker because mortar was applied to the units on both sides of the joint.

Figure 6-2: Typical vertical thin-bed mortar head joint in Shear Wall Pilot Specimen 1

1.1.2 Improved Integrity and Strength of Thin-Bed Mortar Joints in Shear Wall Pilot Specimen 2

After poor bond was encountered during the test on Shear Wall Specimen 1, improved construction procedures were necessary. Shear Wall Specimen 2 was constructed with the help of construction supervisors supplied by Matrix Precast Autoclaved Aerated Concrete (Smyrna, Georgia).

In many aspects, the thin-bed mortar joints of Shear Wall Pilot Specimen 2 behaved better than those of Shear Wall Pilot Specimen 1. Due to improved construction, sliding shear capacity improved along bed joints.

1.1.3 Improved Bond in Bed Joints due to Improved Construction of Pilot Specimen 2

The improved construction consisted of preparing a thicker (more viscous) thin-bed mortar, and then applying it more liberally. The contact surfaces were also more carefully cleaned. In contrast to Pilot Specimen 1, gaps could no longer be seen in the bed joints between panels. Instead, excess mortar was squeezed out when the upper panel was placed (Figure 6-3).

Figure 6-3: Excess thin-bed mortar squeezing out of a bed joint during construction

When the disassembled bed joints of Shear Wall Pilot Specimen 2 were compared to those of Shear Wall Specimen 1, significant improvement could be seen. The ridges that were apparent when the panels of the first wall were disassembled were nonexistent in the second wall. Figure 6-1 shows the lack of contact in many areas of a typical bed joint in Shear Wall Pilot Specimen 1. Figure 6-4 shows the improved contact in a typical bed joint in Shear Wall Pilot Specimen 2, due to improved construction techniques.

Figure 6-4: Typical thin-bed joint in Shear Wall Pilot Specimen 2

1.1.4 Unimproved Bond in Head Joints due to Improved Construction

Improved construction, however, did not improve the performance of head joints. During construction of Pilot Specimen 2, mortar did not consistently squeeze out of these joints, as it did for the bed joints. Instead, in some cases a gap could still be seen between adjacent panels, as with the first specimen. One possible reason for this could be that the shorter panels were not cut sufficiently square. Another reason could be that it is much more difficult to apply enough lateral force to close a vertical gap with the adjacent panel. It is much easier to close a horizontal gap with the help of gravity.

Evidence of the lack of improvement in head-joint contact could be seen after dismantling Shear Wall Pilot Specimen 2. Figure 6-2 shows that some areas had full contact but many ridges existed in the head joints in Shear Wall Pilot Specimen 1. A similar contact surface was found in Shear Wall Pilot Specimen 2, as seen in Figure 6-5.

Figure 6-5: Typical vertical thin-bed mortar head joint in Shear Wall Pilot Specimen 2

1.2 BEHAVIOR OF PANEL REINFORCEMENT

A post-test inspection of Shear Wall Pilot Specimen 2 revealed that its internal drawn-wire reinforcement did not perform ideally. At the ends of the wall where the concrete spalled, the end of the panel had broken off and rotated (Figure 6-6). This rotation occurred when the internal reinforcement slipped with respect to the end of the panel.

This slip occurred for several reasons. First, the concrete that resisted sliding through contact with the vertical end wire, was crushing (Figure 6-7).

Second, the vertical end wire was yielding in flexure (Figure 6-8). Third, after AAC had spalled off the sides of the panel, the layers of reinforcement could spread apart, which reduced the contact between the AAC and the vertical wires, and allowed the panel to rotate. For all of these reasons, the longitudinal reinforcement slid within the panel before yielding.

Figure 6-6: Crack on back of south end of Shear Wall Pilot Specimen 2 showing rotation of end of panel

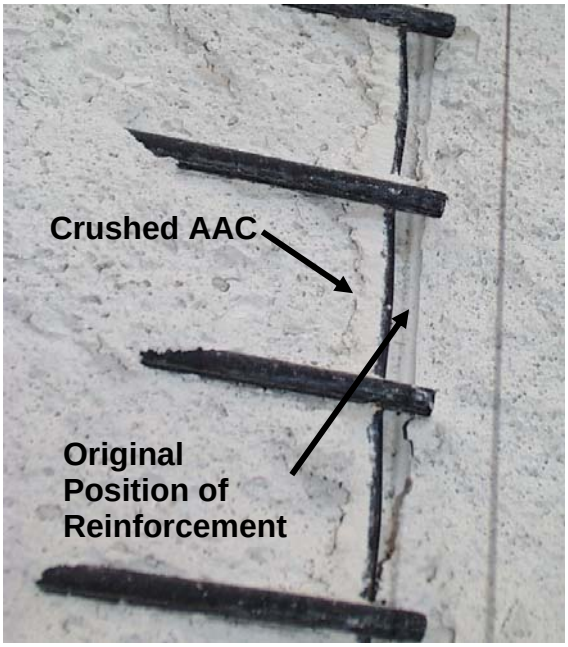

Figure 6-7: Local crushing of AAC around reinforcement

Figure 6-8: Yielding of vertical wire of reinforcement

The behavior mentioned above may represent local effects that may not exist in an actual wall. Nevertheless, it will be monitored in future tests.

1.3 BEHAVIOR OF AAC NEAR LOADING BEAM

1.3.1 Effects of Axial Force

The original loading system was not designed to apply axial loads into the specimens. Instead, an additional beam was going to be added to apply this force. When axial load was added to the specimen to prevent sliding along joints, it had an adverse effect on the specimen. As described in Chapters 4 and 5, the application of axial load by tightening the tie-down rods led to hogging of the loading beam. The deformation of the beam created tensile stresses in the center of the wall and resulted in cracks developing just below the bond beam (Figure 6-9).

Figure 6-9: Tensile crack below bond beam

1.4 EFFECTS OF CLAMPING FORCE

The loading beam also introduced local stresses into the wall through the clamping force. The rods that clamp the steel channels to the wall put local stresses into the bond beam at every clamping point, forming vertical splitting cracks at some of these. By themselves, these cracks are not a problem. Their potential to propagate into the wall and lead to further cracking, however, is a concern.

Recommendations for mitigating these stress concentrations and for further improving construction techniques are presented in Sections 6.5, 6.6, and 6.7.

1.5 PROPOSED CHANGES IN CONSTRUCTION PROCEDURES

The improvements to construction procedures implemented in the construction of Shear Wall Specimen 2 made significant improvements in the bed joints. Thicker thin-bed mortar and better preparation of the panels should continue to be used for future specimens.

To improve head joints, a combination of the methods used in the construction of the first two specimens could be used. The thicker mortar used in Pilot Specimen 2 could be supplemented with the technique of applying a layer of mortar to both faces of the head joint to completely fill the gap between adjacent panels. With the additional mortar in the joint, complete bond along the faces is more likely to be achieved, which will improve the integrity of the head joints.

1.6 PROPOSED CHANGES IN TEST SETUP

After completing two pilot tests and still not reaching the desired wall failure mechanism of web shear cracking, the loading system was re-evaluated, and the following changes were planned to improve the test setup (Figure 6-10)

- increase the magnitude of the axial force, while making its distribution more uniform;
- increase the axial and flexural stiffness of the loading beam;
- reduce the local stresses in the AAC near the loading beam; and
- make other necessary changes due to the redesign of the loading beam.

In this section, each proposed change is discussed and justified.

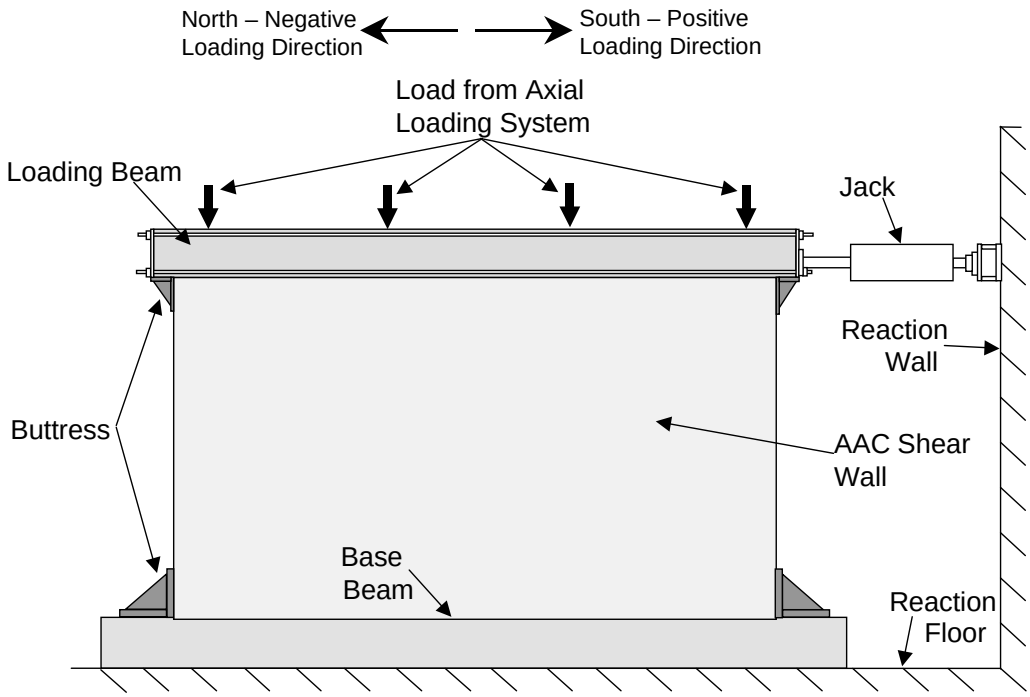

Figure 6-10: Proposed new lateral loading system

1.6.1 Increase the Magnitude of the Axial Force, While Making its Distribution More Uniform

During the test of Shear Wall Pilot Specimen 1, sliding along bed joints accounted for much of the displacement at the top of the wall. To stop the sliding, the axial force will be increased which will increase the shear friction along horizontal joints. With improved bond between the panels, it is probably not necessary to increase the axial force, but it will be increased in any event to around 80 kips (356 kN). This will increase the web shear capacity from 55 kips (245 kN) to 77 kips (343 kN).

When the axial load was increased during the first two pilot tests, all load was applied at the ends of the loading beam, inducing an uneven distribution of axial force along the top of the wall. The first remedy for this problem is to distribute the axial load along the length of the wall at four evenly spaced points (Figure 6-10). The two interior points will have a load of 30 kips (133 kN) each, and the two exterior points, 10 kips (44.5 kN) each. The load applied by the two interior points will be held constant by a load maintainer attached to the hydraulic rams applying the force. The exterior points will not use a load maintainer, and will also act as external reinforcement, as the tie-down rods did in the first two tests. The proposed system for applying the axial load is shown in Figure 6-11.

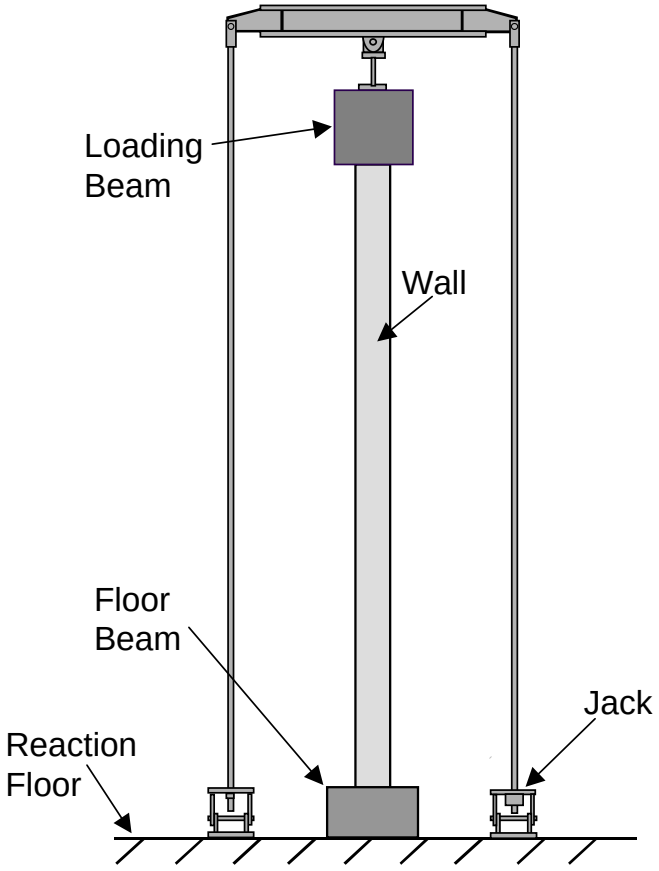

Figure 6-11: Proposed axial loading system

1.6.2 Increase Axial and Flexural Stiffness of Bond Beam

A second problem was that the loading beam was not stiff enough. The most feasible option was to design a concrete beam that would sit on top the wall, and that would be stiff enough to distribute the axial load evenly from the four loading points across the top of the wall. The stiff beam would also help transfer the horizontal shear force evenly along the top of the wall. The new beam has

cross-sectional dimensions of 18 in. (0.457 m) wide and 20 in. (0.508 m) high. It is axially and flexurally much stiffer than the original loading beam.

1.6.3 Reduce Local Stresses in the AAC Near the Bond Beam

The change to a concrete beam (from two steel channels clamped to the sides of an AAC bond beam) also reduces the local stresses from the loading beam. The steel channels put local stresses into the beam at every clamping point, creating vertical splitting cracks at some of these. By changing to a concrete beam resting on top of the wall, and transferring shear force in the mortar joint or by friction, local stress concentrations created by the rods are eliminated.

Local stresses were also induced into the wall at the bearing plates that sat on top of the wall and supported the loading channels. The concrete beam eliminates the need for those bearing plates.

1.6.4 Other Necessary Changes due to the Redesign of the Loading Beam

When the loading beam is changed from two steel channels clamped to the bond beam to a stiff concrete beam, other adjustments will be needed. Since the loading beam will rest on top of the wall instead of being clamped to the bond beam, another way of connecting the loading beam to the wall will be necessary. The first transfer mechanism available is the friction created from the application of the axial force. The axial force will be chosen so that the available frictional resistance will exceed the maximum expected horizontal load.

Even though friction alone would probably be sufficient to prevent the beam from sliding, other precautions are also being taken. First, a conventional mortar joint similar to the joint at the base of the wall will be placed between the top of the AAC wall and the loading beam. As at the bottom of the wall, the mortar will consist of a mixture of Type S PCL mortar and the AAC thin-bed mortar.

Additionally, buttresses will be added. The buttresses at the top of the wall will be very similar to those at the base of the wall, and will be bolted to the ends of the loading beam (Figure 6-10).

Additional improvements are being made to the lower buttresses to allow rotation but not sliding of the wall, which is intended to prevent the pinching behavior evident in the hysteretic loops of Pilot Test 1. The modified buttress detail is shown in Figure 6-12. During Pilot Test 1, hydrostone filled the entire gap between the buttress and the AAC shear wall but this did not allow the wall to rotate. Therefore, in the second test the hydrostone was removed. This, however, allowed the wall to slide along the base, because of the slight gap between the wall and the buttress. The solution is to use a sponge to keep hydrostone out of the bottom of the gap between the wall and the buttress. This will allow the bottom corner of the wall to move vertically without being pinched. Above the sponge, hydrostone will fill the remainder of the gap and will prevent the wall from sliding laterally toward the buttress. Also, a bond breaker will be placed between the hydrostone and the buttress to prevent the buttress from holding down the end of the wall.

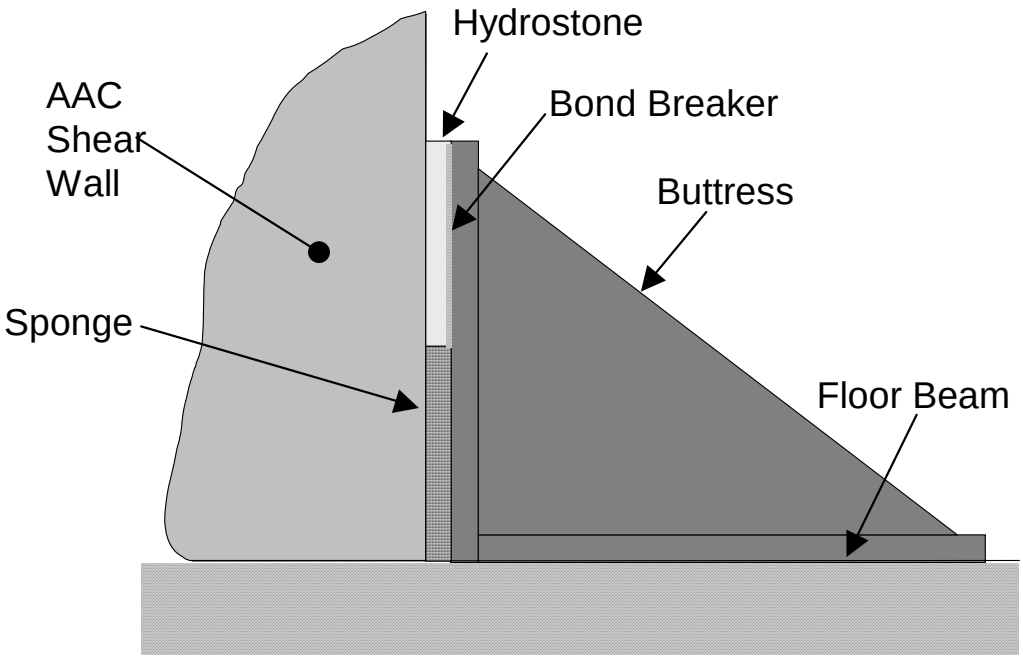

Figure 6-12: Modified buttress detail

Finally, the method of introducing load into the loading beam will have to be modified. The beam will be externally post-tensioned to end plates, and loaded through the end plate (Figure 6-10).

1.7 RECOMMENDATIONS FOR INTERNAL PANEL REINFORCEMENT

Even though slipping of the internal reinforcement might represent local effects that may not exist in an actual wall, some possible modifications are presented here.

The sliding could be stopped by using deformed rather than smooth reinforcement, which would transfer forces from the bar to the AAC along its entire length instead of only at vertical wires. Yielding of vertical wires is probably not a problem and would probably make the specimen more ductile, provided that the AAC does not crush locally.

Another concern is the spreading between the two layers of reinforcement within each panel. One possible remedy would be to provide cross-ties between the reinforcement layers, particularly at the ends of the panels.

CHAPTER 1: SUMMARY, CONCLUSIONS, AND RECOMMENDATIONS

1.1 SUMMARY

The research completed for this thesis involved testing two AAC shear wall pilot specimens under pseudo-static, reversed cyclic loading. These specimens were constructed of horizontal panels, without additional site-installed reinforcement, and without significant axial load. They were designed with a low aspect ratio so that the behavior would be dominated by shear. From the observed behavior and data from the tests, improvements to the construction techniques and testing procedures have been developed, and improvements to existing design models have been made from the preliminary information acquired on the behavior of shear-dominated AAC shear walls.

1.2 CONCLUSIONS

Shear Wall Pilot Specimen 1 and 2 exhibited many kinds of behavior that had been anticipated. They also experienced behaviors that had not been included in the original design models. Most significantly, enough load could not be applied to develop a web shear crack prior to producing other failure mechanisms. The observed behavior not anticipated in the specimens includes:

- separation of the panels along mortar joints;
- tensile cracking around the loading beam; and
- slipping of the internal reinforcement within the panels.

The separation of the panels along the mortar joints was caused by inadequate bond between adjacent panels. Construction techniques were improved prior to building Shear Wall Pilot Specimen 2 which resulted in a higher capacity along the bed joints in this specimen. Further improvements will be made to improve bond in the head joints.

Tensile cracking around the loading beam was caused by high stress concentrations that the loading beam imposed on the wall. The stress concentrations were caused by the post-tensioned rods that clamped the beam to the wall and from the uneven distribution of axial force. The loading beam has been redesigned to eliminate the high stress areas and to distribute both lateral and axial forces evenly across the top of the wall.

The effects of slipping of the internal reinforcement have not yet been determined. The slipping may only be from local effects, which may not actually be present in an actual specimen. This behavior will continue to be monitored in future tests.

The first two pilot specimens have led to improvements in construction techniques, improvements in the testing equipment, and acquisition of preliminary results on the behavior of AAC shear walls. These improvements have led to a redesign of the loading equipment and better construction quality for future specimens which will be used to complete testing of Phase I walls of the project described in Chapter 1.

Initial behavior of low aspect ratio AAC shear walls was observed and is being used to improve current design models, which are based on concrete and masonry provisions.

1.3 RECOMMENDATIONS

The occurrence of local failures prior to web shear cracking has suggested improvements in construction and testing procedures, including:

- using a more viscous thin-bed mortar;
- applying more thin-bed mortar to each joint, particularly the head joints;
- increasing the magnitude and uniformity of the axial force; and
- changing the loading beam to a concrete beam.

These recommendations are justified and more thoroughly discussed in Chapter 6. These improvements reduce the effects that the construction and testing equipment have on the behavior of the walls. Therefore, a more complete set of data will be acquired, which will allow design models to more accurately predict the actual behavior of AAC shear walls, diaphragms, pier elements, cladding and frame infills.

The initial understanding of the behavior of AAC shear walls from the pilot tests, along with the data and information acquired from the remainder of the tests for the research study, will allow design provisions to be developed which will allow AAC to be used safely throughout the United States, including areas of high seismicity.

Appendix A: Sample Calculations for Predicting Major Events

Example of Calculations using Shear Wall Pilot Specimen 1

External Reinforcement

2-1" dia. B7 bars at each end

Constants

$t = 8\,\text{in.}$

$l_w = 240\,\text{in.}$

$h = 148\,\text{in.}$

$\mu = 0.45$

$f_t = 0.043\,\text{ksi}$

$f'_{AAC} = 0.725\,\text{ksi}$

$N = 0\,\text{kips}$

$d = 242.625\,\text{in.}$

$$S_x = \frac{t \cdot l_w^2}{6}$$

$A_v = 0.0597\,\text{in}^2\,(\text{per wire of internal reinforcement})\,(f_y = 60\,\text{ksi})$

$A_s = 0.6\,in^2\ (2-1"\text{dia. B7 bars})\,(f_y = 105\,\text{ksi})$

$$\frac{M}{V} = h$$

Flexural Cracking

$$V_{cr} = \frac{\frac{t \cdot l_w^2}{6}\left(f_t + \frac{N}{t \cdot l_w}\right)}{h} = 22.3\,\text{kips}$$

Web Shear Cracking

$$V_c = \frac{2 \cdot l_w \cdot t}{3} \cdot f_t \cdot \sqrt{1 + \left(\frac{N}{f_t l_w t} \right)} = 55.0 \text{kips}$$

Flexural Shear Cracking

$$V_c = \frac{S_x \cdot \left(f_t + \frac{N}{l_w t} \right)}{\left(\frac{M}{V} - \frac{l_w}{2} \right)} + 0.6 \cdot \sqrt{f'_{AAC}} \cdot td = 142.8 \text{kips}$$

Shear Cracking of Masonry

$$V_m = \left[4 - 1.75 \cdot \left(\frac{M}{V \cdot l_w} \right) \right] \cdot A_n \sqrt{f'_m} + 0.25N = 151.0 \text{kips}$$

Nominal Shear Capacity

$$V_s = \frac{A_v \cdot f_y \cdot d}{s} = 176.1 \text{kips} \quad (h < 0.8 l_w \text{ therefore } d = h)$$

V_c = minimum of web shear cracking and flexural cracking

$$V_n = V_s + V_c = 231.8 \text{kips}$$

Yeild of Flexural Reinforcement

$$V_y = \frac{A_s f_y}{h} \left(d - \frac{c}{3} \right) - \frac{N}{h} \left(\frac{l_w}{2} - \frac{c}{3} \right) = 185.3 \text{kips}$$

Nominal Flexural Strength

$$V_n = \frac{A_s f_y (d - \frac{a}{2})}{h} = 195.7 \text{ kips}$$

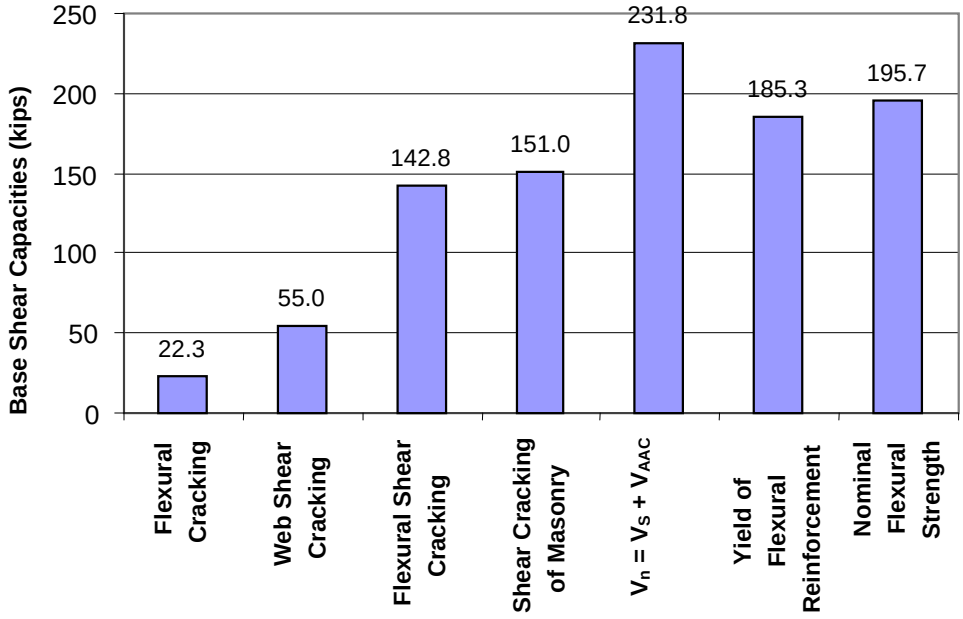

Figure A-1: Summary of Predicted Shear Capacities for Shear Wall Pilot Specimen 1

Appendix B: Histories of Slip at Base of Specimens

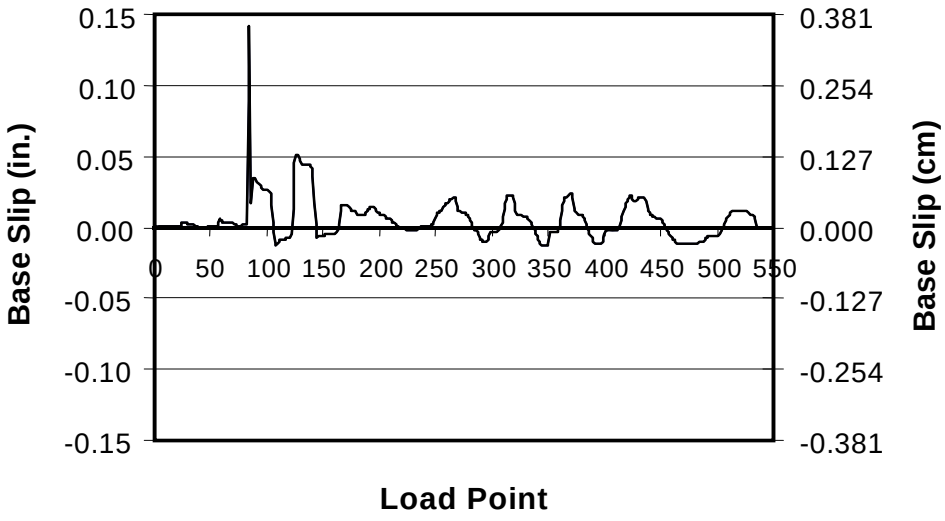

Figure B-1: History of slip at base of Shear Wall Pilot Specimen 1

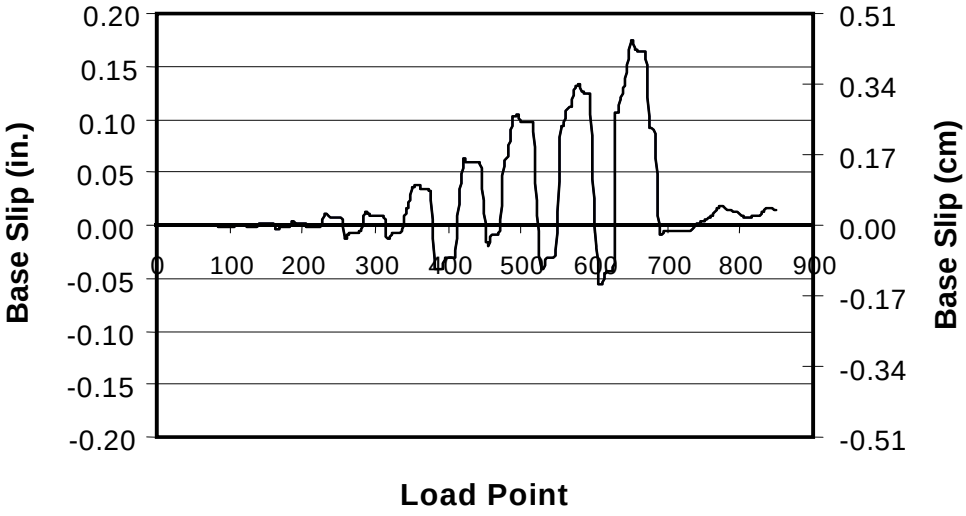

Figure B-2: History of slip at base of Shear Wall Pilot Specimen 2

References

ACI 1999. *Building Code Requirements for Structural Concrete (ACI 318-95) and Commentary (ACI 318R-99),* American Concrete Institute, Farmington Hills, MI.

Al-Shaleh, Moneera and Emmanuel K. Attiogbe. 1997. "Flexural strength characteristics of non-load bearing masonry walls in Kuwait." *Materials and Structures* 30 (June): 277-283.

Chusid, Michael, 2000. "Autoclaved aerated concrete gains a new foothold." *The Concrete Producer* (April): 32-37.

Cardenas, A.E. and D.E. Magura. 1973. "Strength of High-Rise Shear Walls – Rectangular Cross Section." *Paper SP36-7* (ACI Publication SP 36).

de Vekey, R. C. , N. J. Bright, K. R. Luckin, and S. K. Arora. 1986. "Research results on autoclaved aerated concrete blockwork." *The Structural Engineer* 64a (11): 332-340.

Dimitrov, M. 1997. *Carrying out experimental investigations to determine the behaviour and the bearing capacity of Autoclaved Aerated Concrete walls with confining reinforced concrete elements, under reversible horizontal load*. Building Research Institute NISI. Sofia, Bulgaria.

Gerber-Balmelli, Carmen and Peter Marti. 1994. *Versuche an Porenbeton-Mauerwerk.* Institut für Baustatik und Konstruction. Zürich, Switzerland, November.

Hebel 1999a. *Autoclaved Aerated Concrete Masonry Wall Systems.* Product Guide 04225/HEB.

Hebel 1999b. *Introduction to Commercial Building With Hebel Autoclaved Aerated Concrete (AAC)*: Video.

IBC 2000. *International Building Code*, International Code Council, Falls Church, VA.

RILEM 1993. *Autoclaved Aerated Concrete: Properties, Testing and Design*, RILEM Recommended Practice, RILEM Technical Committees 78-MCA and 51-ALC, E & FN Spon, London.

YTONG 1999. *Autoclaved Aerated Concrete*. Product Guide 03404/YTO.